Title	Studies on Preparation and Magnetic Properties of Rare Earth Intermetallic Compounds
Author(s)	泉, 宏和
Citation	大阪大学, 1997, 博士論文
Version Type	VoR
URL	https://doi.org/10.11501/3128997
rights	
Note	

Studies on Preparation and Magnetic Properties of Rare Earth Intermetallic Compounds

（希土類金属間化合物の合成と磁気特性に関する研究）

1997

Hirokazu Izumi

Department of Applied Chemistry
Faculty of Engimeering
Osaka University

Studies on Preparation and Magnetic Properties of Rare Earth Intermetallic Compounds

（希土類金属間化合物の合成と磁気特性に関する研究）
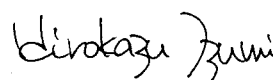
1997

Hirokazu Izumi

Department of Applied Chemistry

Faculty of Engimeering

Osaka University

Preface

The work of this thesis has been carried out under the guidance of Professor Dr. Gin-ya Adachi at Department of Applied Chemistry, Faculty of Engineering, Osaka University.

The object of this thesis is to present a novel preparation process and to improve the properties as commercial permanent magnets for rare earth transition metal intermetallics.

The author wishes that the knowledge obtained in this work provide useful information and suggestion for further development of rare earth-based permanent magnets in the next century.

Hirokazu Izumi

Department of Applied Chemistry

Faculty of Engineering

Osaka University

2-1 Yamadaoka, Suita, Osaka 565

Japan

January 1997

Contents

Chapter 4

Improvement of Magnetic Properties of $Sm_2Fe_{17}C_x$ by Substitution of Co for Fe as Material for Sintered Magnets

Chapter 5

Role of Interstitial Atoms in Magnetic Properties of $Sm_2Fe_{17}X_x$ (X = C or N)

General Introduction

Permanent magnets using rare earth transition metal intermetallics have much stronger magnetic attraction than rare earth free magnets, such as ferrites and alnicos, so that they have contributed to miniaturization in the electronics industry. In recent years, their application spreads widely to the non-electronics industry such as dental or medical industry, and the output has increased year by year. The main compound among the rare earth transition metal intermetallics is $Nd_2Fe_{14}B$ as reported in 1983 by Sagawa et al.[1] The $Nd_2Fe_{14}B$ has a great advantage against the Sm-Co system which has also excellent magnetic properties, since it has a huge energy product (~ 510 kJm^{-3}) and high cost performance (free from Sm and Co). However, defects of the $Nd_2Fe_{14}B$ are low Curie temperature (T_c = 585 K) and low resistivity against oxidation, so that it cannot use in a high temperature condition.

In 1990, Coey et al. have found that Sm_2Fe_{17} absorbs nitrogen to form a new interstitial nitride, $Sm_2Fe_{17}N_x$ (x ~ 3), which has a possibility as the material of high performance permanent magnets in next generation[2]. This compound has a high saturation magnetization (M_s = 1.57 T), a large ideal energy products (BH_{max} = 490 kJm^{-3}) and a high Curie temperature (T_c = 747 K). Furthermore, a carbonitride, $Sm_2Fe_{17}C_xN_y$ ($x+y$ ~ 3), also has excellent magnetic properties[3]. Yang et al. have reported in 1991 that $NdFe_{11}Ti$ also absorbs nitrogen to form the similar interstitial nitride, $NdFe_{11}TiN_x$ (x ~ 1), which has good magnetic properties[4] and an advantage for production cost due to small content of rare earths. For this compound, Ti can be replaced by other elements such as Mo, V, Al and so on. These nitrides are produced by nitridation with N_2 or NH_3-H_2 gas of mother intermetallics made of materials metal. The carbonitrides are also obtained by nitridation of mother carbides which are prepared by carbidation of the intermetallics or melting of materials metal and carbon. Thus, it is necessary for preparation of the nitrides and carbonitrides to use expensive rare earth metals, and the production cost is much higher than those of magnets free from rare earth elements.

These nitrides and carbonitrides decompose at high temperatures (> 900 K), so that they cannot sinter at high temperature as $Nd_2Fe_{14}B$, only use as materials for bonded magnets, which are prepared by bonding of magnetic powder with binders such as resin or metal with low melting point. Magnetization of the bonded magnets is low compared with that of the sintered ones because of

dilution with non-magnetic binders. Hence, we need magnetic powder with excellent magnetic properties for getting the high performance permanent magnets.

This thesis consists of following five chapters.

In **Chapter 1**, a new procedure to prepare the carbonitrides using rare earth dicarbides, which are less expensive than rare earth metals, as a starting material and reducing the amount of rare earth metal use is proposed.

Although the nitrides and carbonitrides have high potential for use as high performance permanent magnets, the magnetic properties of the samples obtained to date are quite low compared with the values expected from the ideal values. **Chapters 2 and 3** deal with the preparation of fine powder of the nitrides with excellent magnetic properties. In **Chapter 2**, a novel procedure to grind the nitrides without deterioration of the magnetic properties is proposed. And **Chapter 3** describes improvement in the oxidation resistance of the fine ground powder obtained in Chapter 2 by means of the surface coating with zinc metal.

Sintered magnets make better use of the magnetic properties of magnetic materials than bonded magnets. Although carbides, $Sm_2Fe_{17}C_x$ ($x < 1$), are one of the candidates for sintered magnets instead of $Nd_2Fe_{14}B$ since they are stable at high temperature, their Curie temperatures and anisotropy field are low and small. Magnetic properties such as magnetization and Curie temperature are generally improved by partial substitution of Co for Fe in rare earth transition metal intermetallic compounds. **Chapter 4** describes the magnetic properties and thermostability of partially Co-substituted carbides, $Sm_2(Fe_{1-x}Co_x)_{17}C_y$, as a material for sintered magnets.

Magnetic properties of Sm_2Fe_{17} are drastically improved by interstitial addition of nitrogen and carbon atoms. However, the role of the interstitial atoms in magnetic properties of $Sm_2Fe_{17}X_x$ (X=C and/or N) is not clarified. In **Chapter 5**, the orbital population of $Sm_2Fe_{17}X_x$ compounds is estimated by use of DV-Xα method, and the role of the interstitial atoms in magnetic properties of $Sm_2Fe_{17}X_x$ is discussed.

List of Publications

[1]   Synthesis of $Sm_2Fe_{17}C_x$ via the Arc Melting of Sm, SmC_2, and Fe

Hirokazu Izumi, Ken-ichi Machida, Daisuke Otsuka, and Gin-ya Adachi

Chemistry Letters, **1993**, 1903-1906.

[2]   Synthesis and Magnetic Properties of $NdFe_{10}Mo_2C_x$ and $NdFe_{10}Mo_2C_xN_y$ Using NdC_2 as a Starting Material

Hirokazu Izumi, Yukitaka Seyama, Ken-ichi Machida, and Gin-ya Adachi

Chemistry Letters, **1994**, 1597-1600.

[3]   Synthesis and Magnetic Properties of $Sm_2Fe_{17}C_xN_y$ Using SmC_2 as a Starting Material

Hirokazu Izumi, Ken-ichi Machida, and Gin-ya Adachi

Journal of Alloys and Compounds, **215**, 245-249 (1994).

[4]   Magnetic Anisotropy of $Sm_2(Fe_{1-x}Co_x)_{17}C_y$

Hirokazu Izumi, Ken-ichi Machida, and Gin-ya Adachi

Japanese Journal of Applied Physics, **34**, L412-L414 (1995).

[5]   Effective Grinding Procedure for $Sm_2Fe_{17}N_x$ Powder with High-Performance Permanent Magnetic Characteristics

Ken-ichi Machida, Atsushi Shiomi, Hirokazu Izumi, and Gin-ya Adachi

Japanese Journal of Applied Physics, **34**, L741-L743 (1995).

[6]   Crystal Structure and Magnetic Properties of $Nd(Fe,M)_{12}C_x$ and $Nd(Fe,M)_{12}C_xN_y$ (M=Mo, Ti, V) Prepared by Cast Method

Hirokazu Izumi, Yukitaka Seyama, Ken-ichi Machida, and Gin-ya Adachi

Journal of Alloys and Compounds, **233**, 231-235 (1996).

3

[7]   High-Performance Characteristics of Bonded Magnets Produced Using $Sm_2Fe_{17}N_x$ Powder Stabilized by Photoinduced Zinc Coating

Hirokazu Izumi, Ken-ichi Machida, Atsushi Shiomi, Masayuki Iguchi, and Gin-ya Adachi

Japanese Journal of Applied Physics, **35**, L894-L896 (1996).

[8]   High-Performance Characteristics of the Bonded Magnets Produced from the $Sm_2Fe_{17}N_x$ Powder Stabilized by Photo-induced Zinc Metal Coatings

Ken-ichi Machida, Hirokazu Izumi, Atsushi Shiomi, Masayuki Iguchi, and Gin-ya Adachi

Proceedings of the 14th International Workshop on Rare-Earth Magnets and Their Applications, Vol. 1, pp. 203-212 (1996).

[9]   Zinc Coatings on $Sm_2Fe_{17}N_x$ Powder by Photoinduced Chemical Vapor Deposition Method

Hirokazu Izumi, Ken-ichi Machida, Masayuki Iguchi, Atsushi Shiomi, and Gin-ya Adachi

in preparation.

[10]   Preparation of $Sm_2Fe_{17}N_x$ Powder and Its Bonded Magnets with High Performance Permanent Magnetic Characteristics

Hirokazu Izumi, Ken-ichi Machida, Atsushi Shiomi, Masayuki Iguchi, Kenji Noguchi, and Gin-ya Adachi

in preparation.

[11]   Estimation for Orbital Population of $Sm_2Fe_{17}X_x$ by DV-Xα Method

Hirokazu Izumi, Ken-ichi Machida and Gin-ya Adachi

in preparation.

List of Supplementary Publication

[1]   Electronic State and Magnetism of the Rare-Earth Carbide GdC$_x$ ($x \approx 0.33$)

Jun Shi, Hirokazu Izumi, Ken-ichi Machida, and Gin-ya Adachi

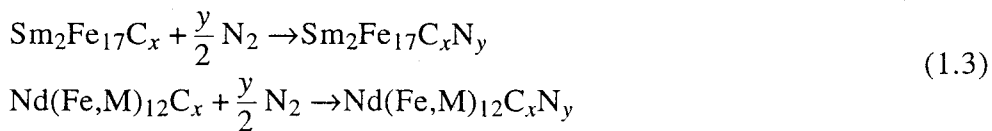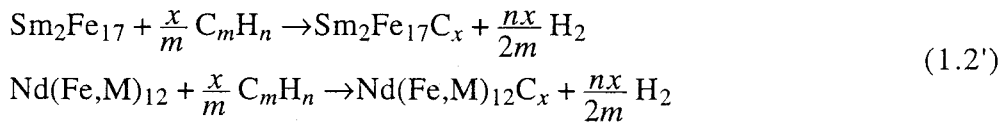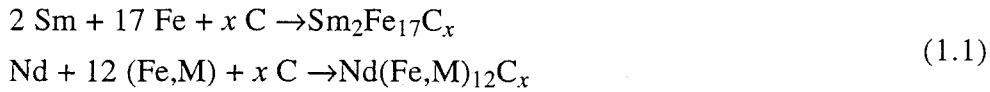*Journal of Alloys and Compounds*, **240**, 156-163 (1996).

Chapter 1

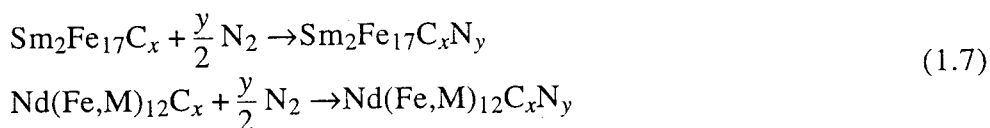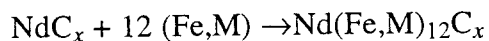# Novel Procedure for Preparation of Carbonitrides Using Rare Earth Dicarbides as a Starting Material

1.1. Introduction

Since Coey et al. reported in 1990[2], an intermetallic compounds, $Sm_2Fe_{17}N_x$ ($x \sim 3$), have attracted much attention as a candidate for new high performance permanent magnets, particularly bonded magnets[5-7], because of its excellent magnetic properties and low thermostability. The saturation magnetization ($M_s = 1.57$ T) of $Sm_2Fe_{17}N_x$ is a match for that of $Nd_2Fe_{14}B$ and the ideal maximum energy product (BH_{max}) attains 490 kJm-3. In addition, the Curie temperature ($T_c = 747$ K) is over 150 K higher than that of $Nd_2Fe_{14}B$, and its anisotropic field ($H_a = 21$ MAm-1) is four times as large as that of $Nd_2Fe_{14}B$.

Kou et al. have tried to prepare the same kind of compounds containing both carbon and nitrogen, $Sm_2Fe_{17}C_xN_y$ ($x+y \sim 3$), which have also excellent magnetic properties and better thermostability than $Sm_2Fe_{17}N_x$[8,9]. The interstitial carbonitrides are usually prepared by nitridation of the mother carbides

$$2 \text{ Sm} + 17 \text{ Fe} + x \text{ C} \rightarrow Sm_2Fe_{17}C_x$$
$$Nd + 12 \text{ (Fe,M)} + x \text{ C} \rightarrow Nd(Fe,M)_{12}C_x \tag{1.1}$$

$$2 \text{ Sm} + 17 \text{ Fe} \rightarrow Sm_2Fe_{17}$$
$$Nd + 12 \text{ (Fe,M)} \rightarrow Nd(Fe,M)_{12} \tag{1.2}$$

$$Sm_2Fe_{17} + \frac{x}{m} C_mH_n \rightarrow Sm_2Fe_{17}C_x + \frac{nx}{2m} H_2$$
$$Nd(Fe,M)_{12} + \frac{x}{m} C_mH_n \rightarrow Nd(Fe,M)_{12}C_x + \frac{nx}{2m} H_2 \tag{1.2'}$$

$$Sm_2Fe_{17}C_x + \frac{y}{2} N_2 \rightarrow Sm_2Fe_{17}C_xN_y$$
$$Nd(Fe,M)_{12}C_x + \frac{y}{2} N_2 \rightarrow Nd(Fe,M)_{12}C_xN_y \tag{1.3}$$

6

from rare earth metal, transition metal and carbon (see Eqs. 1.1 and 1.3)[3] or by nitridation and carbidation of the mother compounds obtained from rare earth metal and transition metal (see Eqs. 1.2 - 1.3)[10]. Therefore, it is in any event necessary for the preparation of them to use the expensive rare earth metal as main raw material, and the production cost is higher than those of the rare earth free permanent magnet materials. Yang et al. have found in 1991 that $NdFe_{11}Ti$ also absorbs nitrogen to form the similar interstitial $NdFe_{11}TiN_x$ ($x \sim 1$) which has good magnetic properties[4]. For this compound, Ti can be replaced by other elements such as Mo, V, Al and so on, and a series of $Nd(Fe,M)_{12}N_x$ (M = Ti, Mo, V, Al etc.) possess a large advantage for the production cost : the Nd metal is less expensive among rare earths and the content per their formula unit (7.7 mol%) is smaller than those of $Sm_2Fe_{17}N_x$/$Sm_2Fe_{17}C_xN_y$ (10.5 mol%) or $Nd_2Fe_{14}B$ (11.8 mol%). On the other hand, rare earth dicarbides, RC_2, are prepared from rare earth oxides and carbon at a low cost (see Eq. 1.4). If we can use RC_2 (R:rare earths) instead of R metal and carbon in order to prepare the carbonitrides, the production cost is expected to be significantly reduced (see Eqs. 1.5 - 1.7).

$$Sm_2O_3 + 7\ C \rightarrow 2\ SmC_2$$
$$Nd_2O_3 + 7\ C \rightarrow 2\ NdC_2 \tag{1.4}$$

$$\frac{x'}{2}\ SmC_2 + \frac{1-x'}{2}\ Sm \rightarrow SmC_{x'}$$
$$\frac{x}{2}\ NdC_2 + \frac{1-x}{2}\ Nd \rightarrow NdC_{x'} \tag{1.5}$$

$$2\ SmC_{x'} + 17\ Fe \rightarrow Sm_2Fe_{17}C_x$$
$$NdC_x + 12\ (Fe,M) \rightarrow Nd(Fe,M)_{12}C_x \tag{1.6}$$

$$Sm_2Fe_{17}C_x + \frac{y}{2}\ N_2 \rightarrow Sm_2Fe_{17}C_xN_y$$
$$Nd(Fe,M)_{12}C_x + \frac{y}{2}\ N_2 \rightarrow Nd(Fe,M)_{12}C_xN_y \tag{1.7}$$
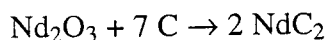
In the work described in this chapter, the rare earth interstitial carbonitrides, $Sm_2Fe_{17}C_xN_y$ and $Nd(Fe,M)_{12}C_xN_y$ (M = Mo, Ti and V) were prepared by the cast method using SmC_2 and NdC_2 as raw materials and by the subsequent nitridation. The x-ray diffraction (XRD) patterns, carbon and nitrogen

7

contents, and magnetic properties of the resulting materials were compared with those of the carbonitrides prepared by means of the conventional methods without RC_2.

1.2. Experimental Details

Appropriate amounts of rare earth oxides, R_2O_3 (purity, 99.9%) and carbon powder (reagent grade) were intimately mixed and pressed to a button-like pellets. The mixture of Sm_2O_3 and carbon was heated on an alumina boat at 1923K for 7h in a stream of Ar (100 cm^3min^{-1}), and NdC_2 was obtained by heating at 1923 K for 7 h in vacuum ($< 8 \times 10^{-5}$ Pa). It was necessary for preparation of the single phase of oxygen-free dicarbides to add 10 or 20 mol% excess of carbon to the stoichiometry composition of the dicarbides. An intermediate material, RC_x with $0 < x < 1.5$ was prepared by arc melting of the various amounts of RC_2 and rare earth metals in an Ar atmosphere (ca. 65 kPa).

The mixtures of RC_2 or RC_x, Fe (99.5%) and M [Ti (99.9%), Mo (99.95%), or V (99.9%)] with a molar ratio of the stoichiometric composition were melted in a similar manner as the preparation procedure for RC_x, followed by annealing on a Ta boat in a purified Ar atmosphere at 1173 - 1373 K for 48 - 168 h. The 5 or 20 mol% excess addition of the RC_2 (RC_x) materials was to compensate for the evaporation loss of the rare earth elements during the melting and annealing treatments. The resulting carbides were ground in inert atmosphere to a particle size < 50 μm, and the thermal or plasma nitridation process was applied to them under the same conditions reported elsewhere[11,12]. The resulting carbides and carbonitrides were identified on the basis of XRD measurements, and their carbon and nitrogen contents were determined by uses of carbon and nitrogen analyzers (Kokusaidenki COULOMATIC-C, Horiba EMGA-550). The Curie temperatures (T_c) were evaluated from the temperature dependence curves of magnetization which were measured by use of a magnetic balance (Shimadzu MB-11) in a magnetic field of 13.4 kAm^{-1} and a temperature range of 300 - 800 K.

1.3. Results and Discussion

1.3.1. Preparation of RC_2 and RC_x

Figure 1.1 shows the XRD patterns of the SmC_2 compounds prepared from the mixtures with two compositional ratios of Sm_2O_3 and carbon, *viz.* $Sm_2O_3 : C = 1 : 7$ (stoichiometric) and $1 : 7.7$ (10 mol% carbon excess). For the sample obtained from the stoichiometric mixture (pattern a), the XRD profile was still mixed with some peaks assigned to that of Sm_2O_3. However, all the peaks of pattern b (the sample from the mixture with 10 mol% excess carbon) were almost completely assigned on the basis of tetragonal lattice reported on SmC_2, and furthermore the calculated lattice parameters (a = 3.76 and c = 6.30 Å) were in good agreement with the reported values (a = 3.770 and c = 6.331 Å)[13]. The observed carbon content of the latter carbide was 14.0 wt% (found value), which was similar to the calculated one (13.8 wt%). Therefore, the SmC_2 compound obtained from mixture with 10 mol% excess carbon was judged to form as a single phase. The small amount of unreacted carbon may still exist in the grain boundary of SmC_2 particles as amorphous or fine particle crystalline carbon.
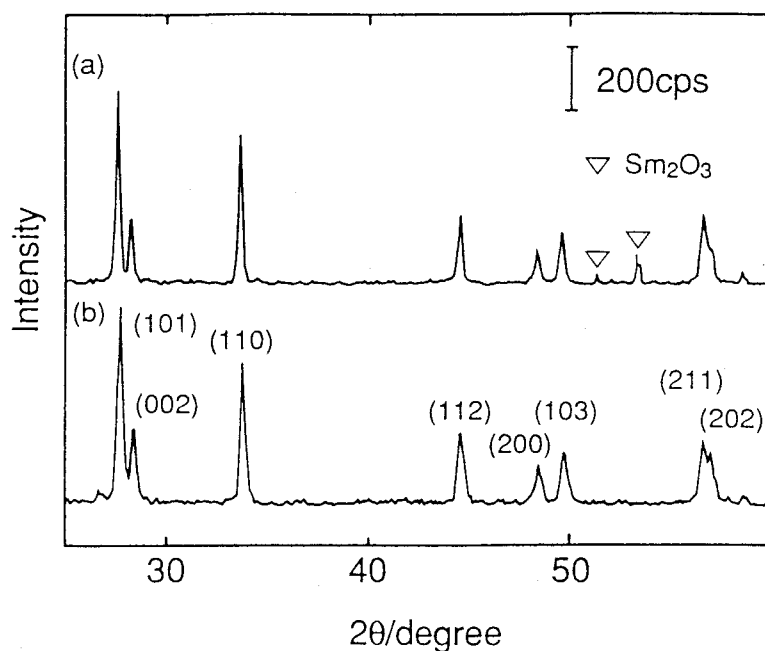

Figure 1.1. XRD patterns of SmC_2 samples prepared from the starting material mixture of Sm_2O_3 containing (a) 0 mol% and (b) 10 mol% excess C.
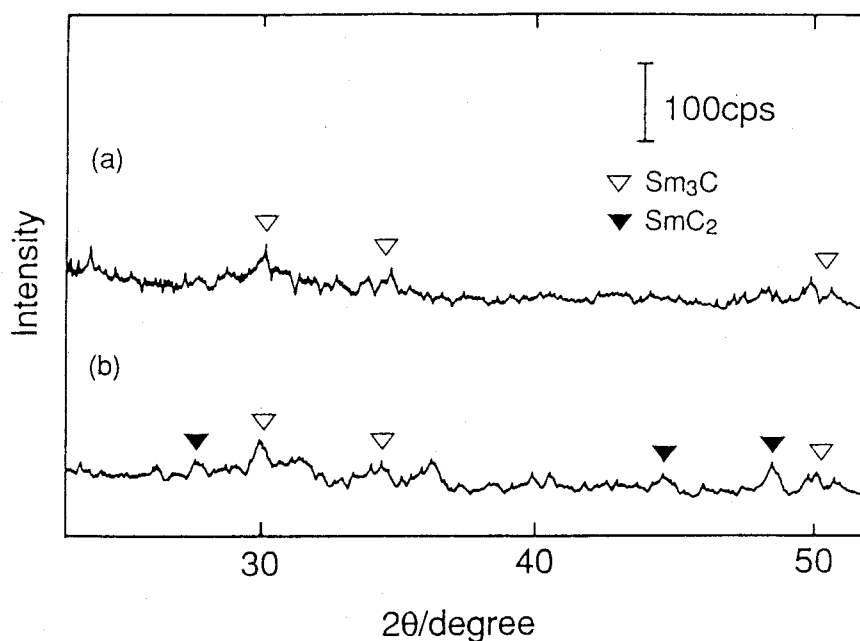
Figure 1.2. XRD patterns of SmC_x samples obtained from SmC_2 and Sm metal, with overall analytical composition (a) $SmC_{0.30}$ and (b) $SmC_{0.58}$.

The XRD patterns of SmC_x are shown in Fig. 1.2. The profile of $SmC_{0.30}$ sample (pattern a) consisted of several broad peaks, which were almost assigned according to the cell data for Sm_3C (cubic, a = 5.172 Å)[14] in spite of the low cristallinity of the sample. However, the $SmC_{0.58}$ sample provided the mixed XRD profile of Sm_3C, SmC_2 and unidentified phase (pattern b). This indicates that the single phase compound is not obtained in the range of $x > 0.5$ (or Sm / SmC_2 ratio < 3), although Sm_3C has been reported to exist over a wide solid solubility range of carbon because of the formation of defects in the lattice[15]. Furthermore, the homogeneous melt could not be obtained in the range of $x > 1$ (Sm / SmC_2 ratio < 1).

The same results were obtained in the case for NdC_2 and NdC_x.

1.3.2. Preparation of the R-Fe(-M)-C System

(a) Preparation Using RC_2

The XRD patterns of the samples obtained from SmC_2 and Fe, and NdC_2, Fe, and Mo are shown in Fig. 1.3 and 1.4, respectively. For Sm-Fe-C system, all peaks were completely assigned to α-Fe and SmC_2 according to the cell data (cubic, a = 2.8664 Å for α-Fe[16] and tetragonal, a = 3.770 and c =
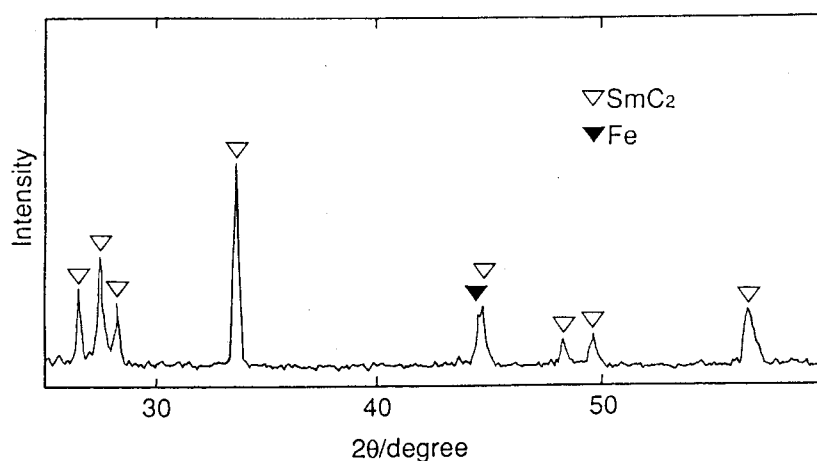
Figure 1.3. XRD patterns of the samples obtained from SmC_2 and Fe metal, with overall analytical composition $Sm_2Fe_{17}C_{4.6}$.
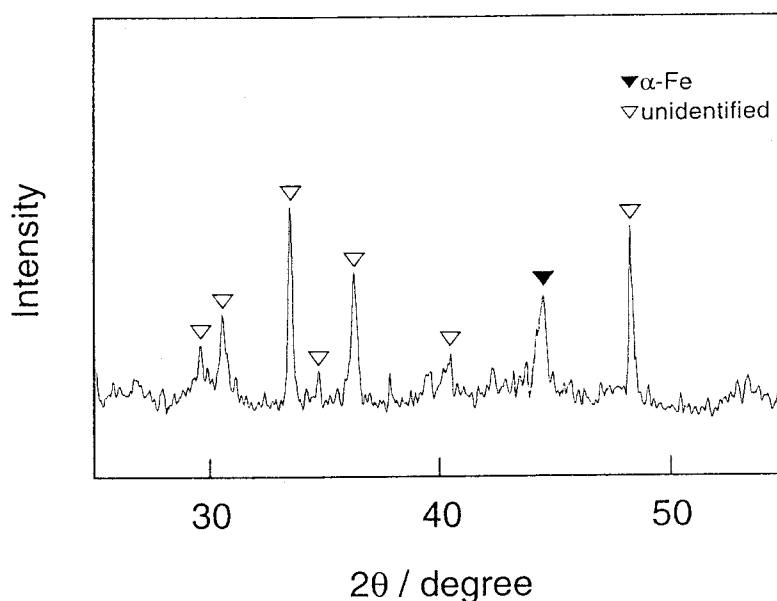

Figure 1.4. XRD patterns of the sample obtained from NdC_2, Fe and Mo metal.

6.331 Å for SmC_2[13]). The profile shown in Fig 1.4 consists of the peaks derived from α-Fe and unidentified phase. Since the carbon atoms generally share the 9e sites of the Th_2Zn_{17}-type crystal lattice (space group R-3m) and the 2b sites of the $ThMn_{12}$-type crystal lattice (space group I4/mmm), the carbon content (x) should be respectively less than 3 and 1. According to Eq. 1.6, the carbon content per formula unit is expected to be the value of $x = 4$ and 2 which is out of the crystallographic limitation. Therefore, the excess carbon is concluded to depress the formation of $Sm_2Fe_{17}C_x$ and

11

$NdFe_{10}Mo_2C_x$ crystal lattice. Similar results to this were obtained in the other Nd-Fe-Ti-C and Nd-Fe-V-C systems.

Jeitschko et al. have reported that the mixtures of RC_2 and Fe give the compounds represented as formula units of $RFeC_2$ and R_2FeC_4 for heavy rare earths, which are formed by a peritectic reaction of them[17,18]. Also, Stadelmaier et al. have reported that GdFeC and $Gd_4Fe_4C_7$ phase exists in Gd-Fe-C system[19]. Hence, some compounds like these may be formed rather than $Nd(Fe,M)_{12}C_x$ in the Nd-Fe-M-C system, although the XRD pattern of the unidentified phase obtained here is different from the patterns of them.

(b) Preparation Using RC_x

A series of XRD patterns of $Sm_2Fe_{17}C_x$ (x = 0, 0.75 and 1.8) were shown in Fig. 1.5. The samples with x = 0 and 0.75 provided only the XRD patterns originated from the rhombohedral Th_2Zn_{17}-type crystal lattices of Sm_2Fe_{17} and $Sm_2Fe_{17}C_x$ (a = 8.55 - 8.63 and c = 12.4 - 12.5 Å for the hexagonal setting)[8,9]. Therefore, one can judge that these samples are formed as pure materials with the Th_2Zn_{17}-type structure. Particularly, the XRD pattern of $Sm_2Fe_{17}C_{0.75}$ was shifted to the low degree side of 2θ compared with that of Sm_2Fe_{17}. This means that the crystal lattice of $Sm_2Fe_{17}C_{0.75}$ is expanded by the carbon atoms which are introduced to the interstitial 9e sites of Sm_2Fe_{17} crystal lattice. The lattice parameters of Sm_2Fe_{17} and $Sm_2Fe_{17}C_{0.75}$ were listed in Table 1.1, together with the values of Curie temperature which were evaluated from the temperature dependence of magnetization given in Fig. 1.6. For $Sm_2Fe_{17}C_{0.75}$, the T_c value ($\approx$ 500 K) was elevated compared with that of Sm_2Fe_{17} (425 K) as the cell volume increased by 1.4%.

On the other hand, the mixture of $SmC_{0.58}$ and Fe metal provided an entirely different XRD profile from that of the $Sm_2Fe_{17}C_x$ phase, which consisted of α-Fe and an unidentified phase (see the pattern c in Fig. 1.5). The latter unidentified phase may be assigned as Sm-rich compounds in the Sm-Fe-C system such as SmFeC or $Sm_4Fe_4C_7$, which has been found in the Gd-Fe-C system[20]. The high T_c value observed (> 800K) was due to the presence of the α-Fe phase with T_c = 1043K. A number of attempts for the preparation of $Sm_2Fe_{17}C_x$ have been demonstrating that, besides the crystallographic limitation to carbon content described above, a different kind of limitation apparently

exists and the criterion of carbon content is judged to be $x \approx 1$[21], although the carbon atoms generally

share the 9e sites of the Th_2Zn_{17}-type crystal lattice. Therefore, it is understood that the carbon content

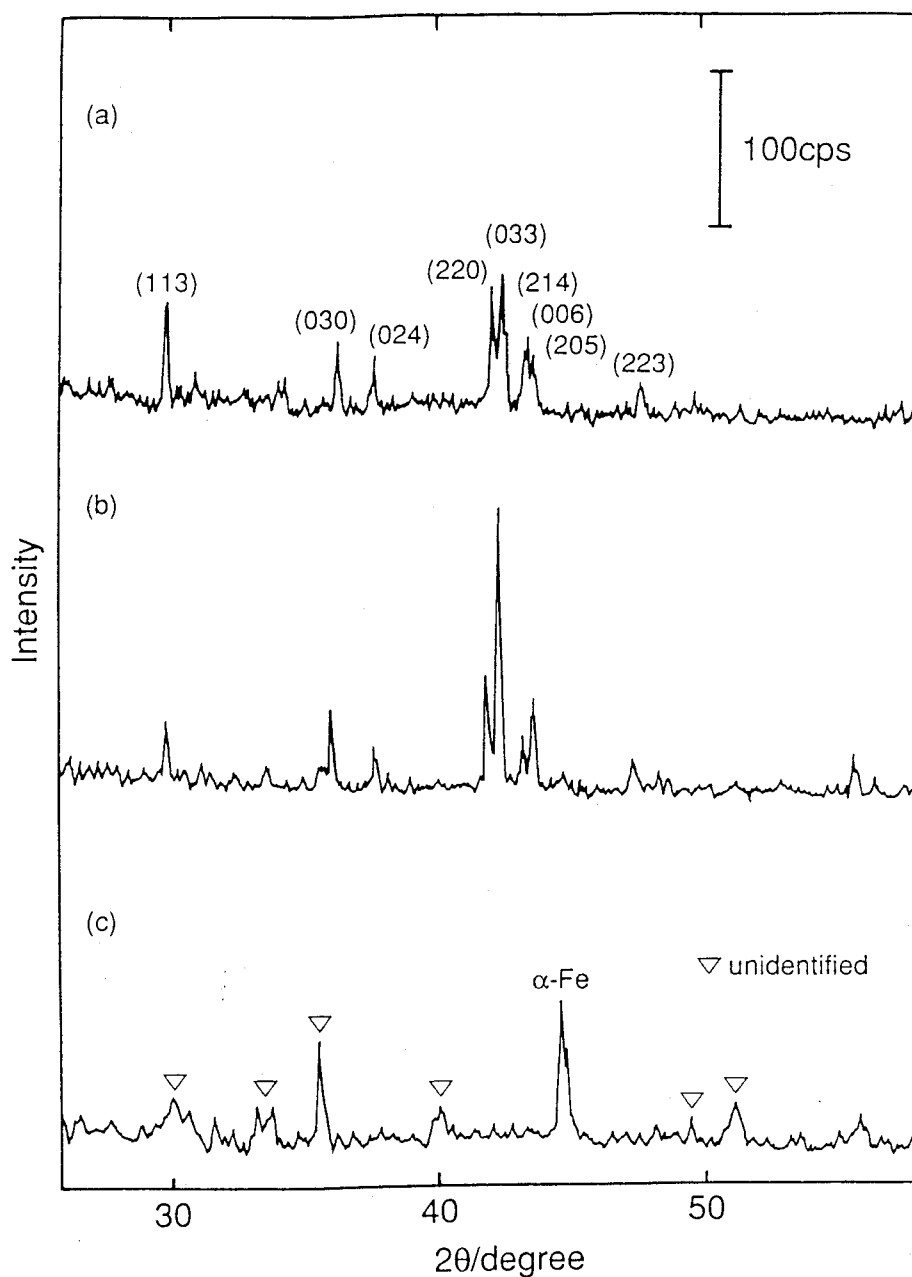of the sample with $x \approx 1.8$ is too high to form the crystal lattice of $Sm_2Fe_{17}C_x$.

Figure 1.5. XRD patterns of $Sm_2Fe_{17}C_x$ materials obtained from $SmC_{x'}$ (x'=0, 0.30, 0.58) and Fe metal, with overall analytical composition (a) x=0, (b) x=0.75 and (c) x=1.8.

13

Table 1.1. Lattice parameters and Curie temperatures of the resulting compounds in the Sm-Fe-C and Sm-Fe-C-N systems.

Composition	Phase[a]	a (Å)	c (Å)	V (Å^3)	T$_c$ (K)
Sm_2Fe_{17}	Th_2Zn_{17}	8.55	12.4	788	425
$Sm_2Fe_{17}C_{0.75}$	Th_2Zn_{17}	8.62	12.4	797	500
$Sm_2Fe_{17}C_{1.8}$	α-Fe + unidentified	-	-	-	> 800
$Sm_2Fe_{17}C_{0.89}N_{2.66}$	Th_2Zn_{17}	8.73	12.7	838	725

[a]Based on XRD patterns.
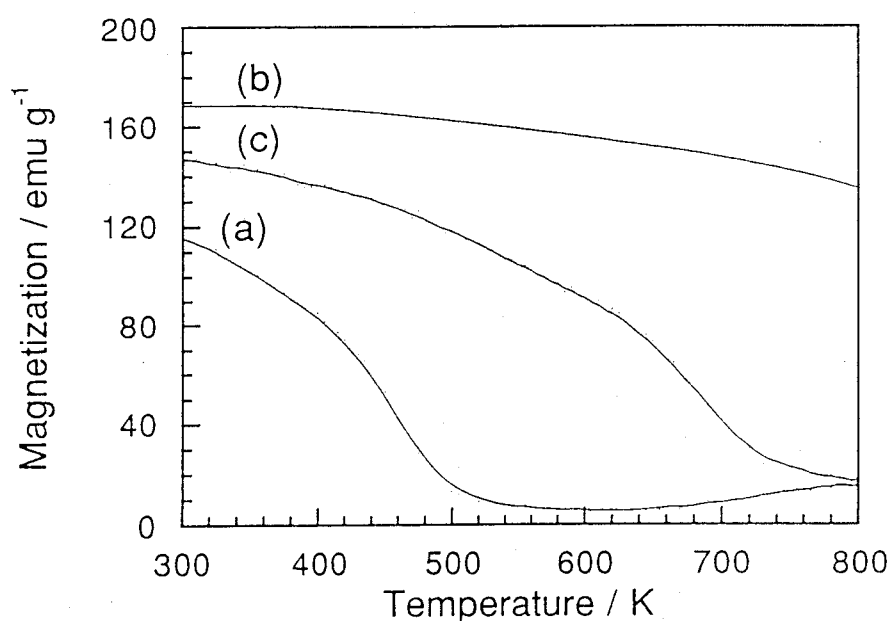
Figure 1.6. Temperature dependence of the magnetization of $Sm_2Fe_{17}C_x$ and $Sm_2Fe_{17}C_xN_y$: (a) $Sm_2Fe_{17}C_{0.75}$; (b) $Sm_2Fe_{17}C_{1.8}$; (c) $Sm_2Fe_{17}C_{1.00}N_{2.49}$.

The XRD patterns of $NdFe_{10}Mo_2C_x$ obtained from the NdC_x with various x values, Fe and Mo metal are shown in Fig. 1.7, and the lattice parameters of $Nd(Fe,M)_{12}C_x$ are listed in Table 1.2. For $NdFe_{10}Mo_2C_{0.25}$ (pattern b), the peaks observed were completely assignable to a $ThMn_{12}$-type crystal structure. In addition, the XRD pattern was shifted to a low degree side in 2θ compared with that of $NdFe_{10}Mo_2$ (pattern a), and this means that the unit cell was expanded with the carbon addition. These results suggest that the crystal lattice of $NdFe_{10}Mo_2C_x$ is expanded by the carbon atoms introduced at

the 2b sites interstitially. Furthermore, the XRD patterns of $NdFe_{10}Mo_2C_{0.50}$ and $NdFe_{10}Mo_2C_{0.80}$

(patterns c and d) were shifted to the much lower sides in 2θ, but the crystallinity was reduced and led

to the appearance of some unidentified peaks. Even though the crystallographic limitation of carbon

content per formula unit of $NdFe_{10}Mo_2C_x$ is $x \leq 1$, the compounds with a $ThMn_{12}$-type crystal structure

cannot be obtained as the single phase in the high carbon content region $x > 0.5$. This is because the 2b

site of a $ThMn_{12}$-type structure is too small to allow carbon atoms to share fully at the sites. Also, the
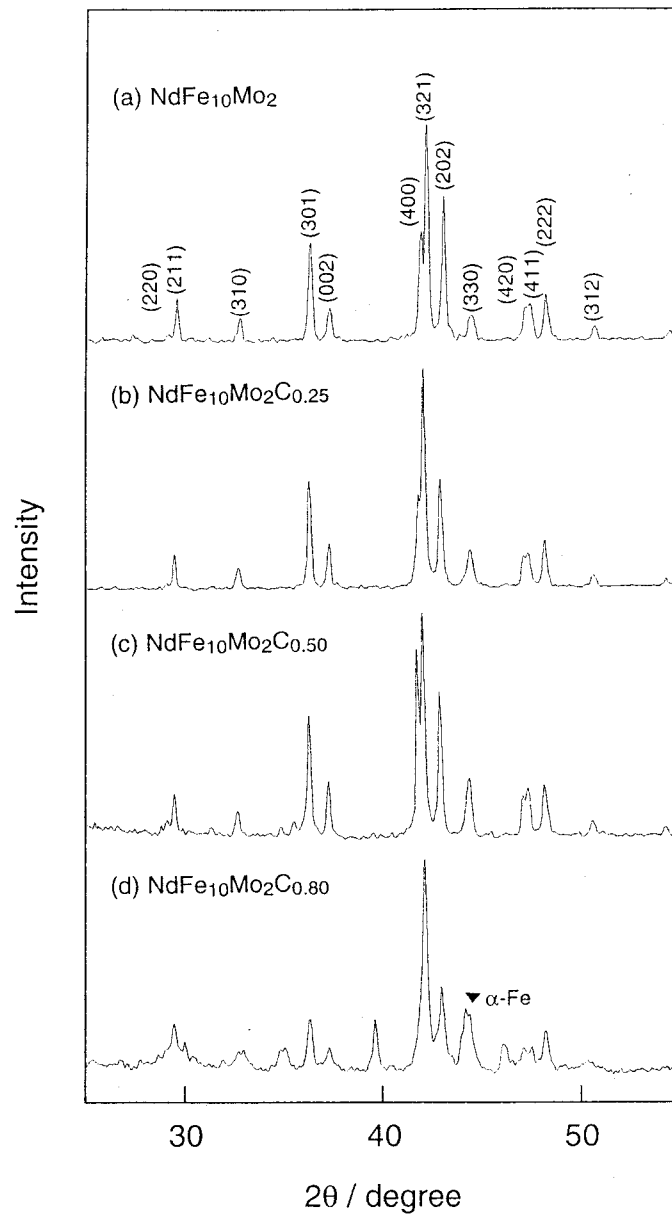

Figure 1.7. XRD patterns of the sample obtained from NdC_x, Fe and Mo metal.

15

Table 1.2. Structural data and Curie temperature (T_c) for $Nd(Fe,M)_{12}C_x$ and $Nd(Fe,M)_{12}C_xN_y$ compounds

Composition	Lattice parameter[a]		Cell volume V (nm^3)	$\Delta V/V_0$[b] (%)	Curie temperature T_c (K)
	a (nm)	c (nm)			
$NdFe_{10}Mo_2$	0.862	0.481	0.357	–	400
$NdFe_{10}Mo_2C_{0.25}$	0.864	0.482	0.360	0.62	440
$NdFe_{10}Mo_2C_{0.50}$	0.860	0.487	0.360	0.73	450
$NdFe_{10}Mo_2C_{0.80}$	0.856	0.491	0.360	0.73	460
$NdFe_{10}Mo_2C_{0.25}N_{0.30}$	0.864	0.485	0.363	1.46	510
$NdFe_{11}Ti$	0.859	0.479	0.353	–	550
$NdFe_{11}TiC_{0.25}$	0.855	0.483	0.353	-0.08	550
$NdFe_{11}TiC_{0.50}$	0.859	0.478	0.352	-0.25	545
$NdFe_{11}TiC_{0.25}N_{0.31}$	0.864	0.482	0.360	1.90	660
$NdFe_{10}V_2$	0.855	0.477	0.349	–	580
$NdFe_{10}V_2C_{0.25}$	0.856	0.477	0.350	0.20	600
$NdFe_{10}V_2C_{0.50}$	0.856	0.478	0.350	0.32	605
$NdFe_{10}V_2C_{0.25}N_{0.31}$	0.861	0.478	0.354	1.49	685

[a]With an error of ±0.001 nm

[b]V_0 is the unit cell volume for $Nd(Fe,M)_{12}$.

XRD patterns of $NdFe_{10}V_2C_x$ prepared from NdC_x, Fe, and V were slightly shifted to a low degree side in 2θ by reason of the carbon introduced to the interstitial sites of the lattice as well as $NdFe_{10}Mo_2C_x$.

Cell volumes of the resulting $Nd(Fe,M)_{12}C_x$ (M = Mo and V) materials were increased with increase of their carbon content. However, the cell volume of the $NdFe_{11}TiC_x$ was inversely decreased with increase of the carbon content. These suggest that all carbon do not introduced to the 2b sites interstitially. Yang et al. have reported that the carbon atoms occupy the 8i sites rather than the 2b sites and the unit cell volume decreases as the carbon content increases for tetragonal $RFe_{11-x}TiC_x$ (R = Sm, Gd, Dy, Ho, Er and Y) prepared by arc melting on the basis of XRD patterns[22]. Therefore, some carbon atoms likely share the 8i sites in $Nd(Fe,M)_{12}C_x$.

16

1.3.3. Preparation of the R-Fe(-M)-C-N System

The $Sm_2Fe_{17}C_xN_y$ sample obtained by nitridation of $Sm_2Fe_{17}C_x$ also provided the XRD pattern assigned to the Th_2Zn_{17}-type crystal structure which was shifted to the low degree side of 2θ compared with that of Sm_2Fe_{17}. The magnitude of the shift depended on the temperature and time for nitridation. The cell volume of $Sm_2Fe_{17}C_{0.89}N_{2.66}$ listed in Table 1.1 was increased by 8.1% compared with Sm_2Fe_{17}. This indicates that nitrogen atoms are also located at the interstitial 9e sites of the Sm_2Fe_{17}
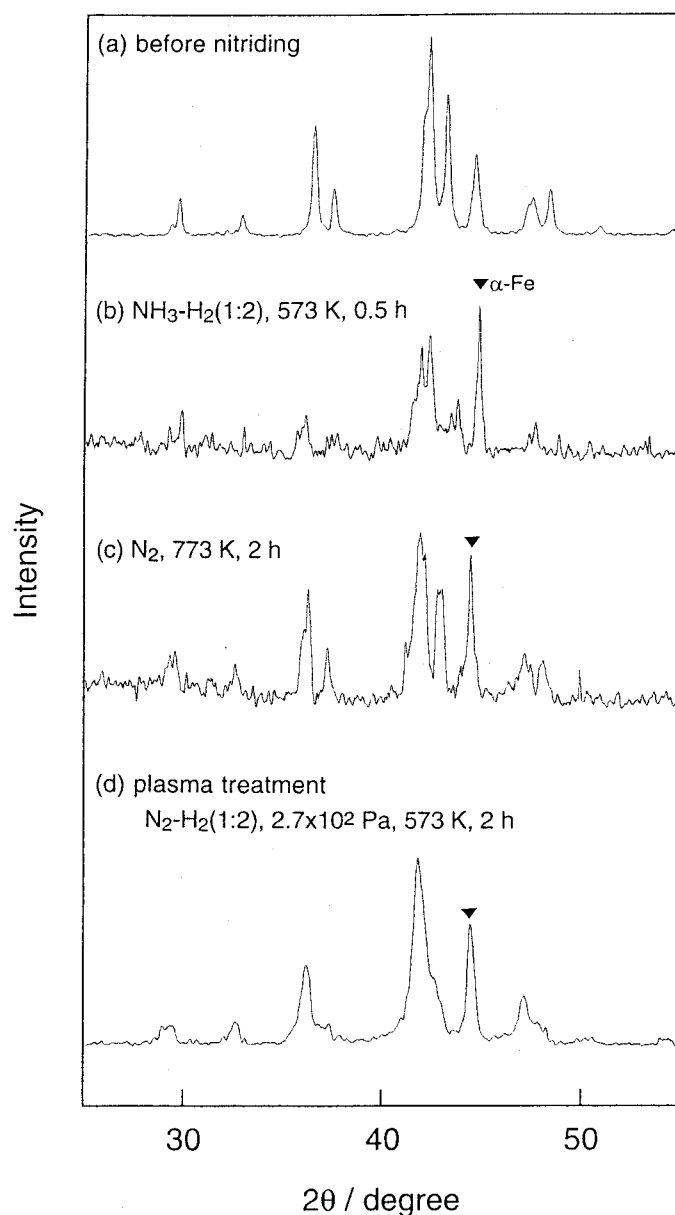

Figure 1.8. XRD patterns of nitrogenized $NdFe_{10}Mo_2C_{0.25}$.

crystal lattice.

For the sample heated in a mixed gas of NH_3-H_2 (molar ratio = 1 : 2) at 573 K for 0.5 h (Fig. 1.8, pattern b), the peaks of XRD pattern assigned to $NdFe_{10}Mo_2C_{0.25}N_x$ appeared together with those of raw compound, $NdFe_{10}Mo_2C_{0.25}$. However, the thermal decomposition to $Nd(C,N)_x$ and α-Fe seriously took place under the conditions of higher temperature and longer heating time, and hence we were not able to get the carbonitride as the single phase. This is due to the high reactivity of the NH_3-H_2 mixed gas. In contrast with the case of the NH_3-H_2 mixed gas, the nitridation of $NdFe_{10}Mo_2C_{0.25}$ with N_2 gas hardly performed even at 723 K, and slightly occured at 773 K (see Fig. 1.8, pattern c). However, since the high temperature treatment on accounts of the low reactivity of N_2 gas led to the decomposition, therefore the thermal nitridation using N_2 gas was also unsuitable for the preparation of $Nd(Fe,M)_{12}C_xN_y$. The plasma nitridation can proceed at the lower temperature than that of the thermal nitridation[12]. The XRD pattern of $NdFe_{10}Mo_2C_{0.25}$ after the plasma treatment is shown in Fig. 1.8 (pattern d). The pattern was shifted to a lower degree side in 2θ than that of the corresponding carbides with little decomposition. The similar results were obtained in $NdFe_{11}TiC_{0.25}$ and $NdFe_{10}V_2C_{0.25}$. Therefore,

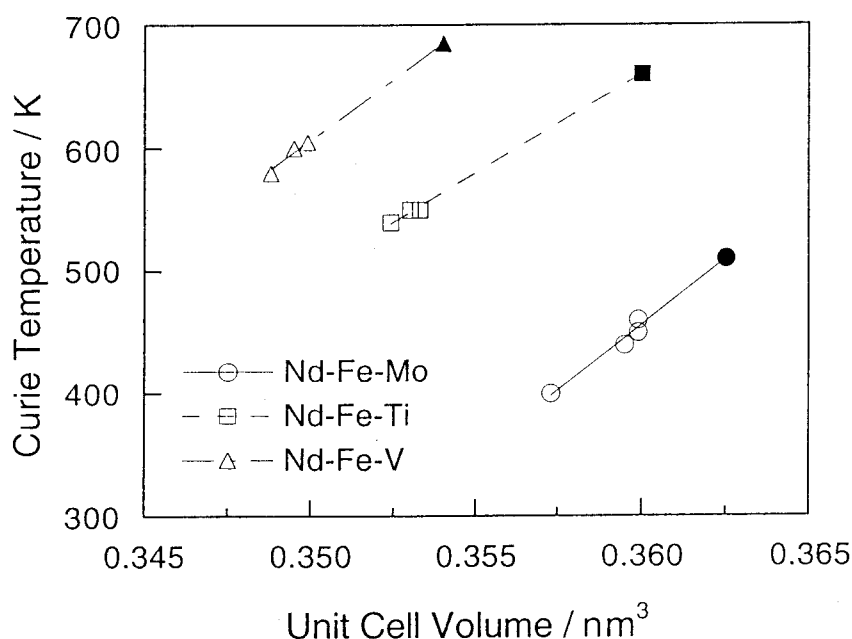**Figure 1.9.** Cell volume expansion dependence of the Curie temperature of $Nd(Fe,M)_{12}C_x$. open: carbides obtained here; full: carbonitrides obtained here.

the plasma nitridation performs efficiently compared with the thermal nitridation for $Nd(Fe,M)_{12}C_x$.

The Curie temperature increased in proportion to the unit cell volume (see Table 1.1 and Fig. 1.9). Generally, the Curie temperatures of R-Fe systems depend upon the Fe-Fe interaction[23]. Therefore, the T_c elevation results from the enhancement of the exchange interaction between Fe atoms due to the elongation of Fe-Fe interatomic distance in the crystal lattice by the introduction of carbon or nitrogen atoms, and the T_c values of the nitrides and carbonitrides are independent of a species of interstitial elements.

The saturation magnetization (M_s), residual magnetization (B_r) and coercive force (H_{cj}) of the $Sm_2Fe_{17}C_{0.89}N_{2.66}$ sample obtained above are listed in Table 1.3, together with those of the sample obtained by the conventional method using Sm, Fe and C elements ($Sm_2Fe_{17}C_{1.00}N_{2.49}$). All the values of M_s, B_r and H_{cj} of the former sample were almost similar to those of the latter one. Therefore, it is concluded that the $Sm_2Fe_{17}C_xN_y$ material with the same level of magnetization characteristics as the sample prepared by the conventional technique can be produced by the cast method using SmC_2 as one of raw materials instead of Sm metal and carbon.

Table 1.3. Magnetic properties of $Sm_2Fe_{17}C_xN_y$.

Composition	Magnetic properties		
	M_s (T)	B_r (T)	H_{cj} (MAm^{-1})
$Sm_2Fe_{17}C_{0.89}N_{2.66}$	1.04	0.93	0.27
$Sm_2Fe_{17}C_{1.00}N_{2.49}$[a]	1.11	0.80	0.29

[a]This material was prepared by arc melting appropriate amounts of Sm, Fe and C.

1.4 Conclusions

Although the direct reaction between RC_2 and Fe metal does not produce Th_2Zn_{17}-type or $ThMn_{12}$-type compounds, the $Sm_2Fe_{17}C_x$ ($x < 1$) and $Nd(Fe,M)_{12}C_x$ ($x < 0.5$) in the low concentration region of carbon are obtained by use of RC_x as a source for rare earths and carbon. The further nitridation of $Sm_2Fe_{17}C_x$ produces the $Sm_2Fe_{17}C_xN_y$ compound which possesses good magnetic properties as

19

well as the same material prepared by the conventional technique. The plasma nitridation performs efficiently compared with thermal nitridation for $Nd(Fe,M)_{12}C_x$. The T_c values of $Nd(Fe,M)_{12}C_xN_y$ are depend upon the corresponding unit cell volume and independent of a kind of interstitial atoms in a similar manner as observed on the $Nd(Fe,M)_{12}C_x$ and $Nd(Fe,M)_{12}N_x$ samples prepared by the conventional method.

The use of RC_2 as the raw material instead of rare earth metal and carbon may contribute to the reduction of production cost for the rare earth transition metal intermetallic carbonitrides.

Chapter 2

Effective Grinding of $Sm_2Fe_{17}N_x$ Powder in Organic Solutions with a Surfactant

2.1. Introduction

The coercivity mechanism of $Sm_2Fe_{17}N_x$ and $Sm_2Fe_{17}C_xN_y$ is controlled by nucleation process[24], so that the microcrystalline of $Sm_2Fe_{17}N_x$ and $Sm_2Fe_{17}C_xN_y$ possesses high coercivity. Rani et al.[25] have found that $H_{cj} = 1.8$ MAm^{-1} is observed on the $Sm_2Fe_{17}N_x$ powder prepared by means of rf sputtering and Katter et al. have reported that a nitrogenized $Sm_{12.5}Fe_{87.5}$ sample obtained by a rapid quenching technique provides a value of $H_{cj} = 2.4$ MAm^{-1}[26]. Mechanical alloying method has been also demonstrated to provide a high H_{cj} value of 2.4 MAm^{-1} reported by Kou et al[27]. However, since these samples are magnetically isotropic or contain some soft magnetic phases, $e.g.$ α-Fe and Sm_2Fe_{17}, the remanence (B_r) values of them are quite low. Magnetically anisotropic powder with high B_r value is able to be obtained by fine grinding of $Sm_2Fe_{17}N_x$ bulk. The grinding process is very important in order to prepare the powder sample with high B_r and H_{cj} values of $Sm_2Fe_{17}N_x$, since they depend upon not only the particle size but the surface and bulk conditions of finely ground powder. The ball milling technique performed in the presence of a solvent produces fine powder materials without including any extra strain during the grinding process. However, powder particles of samples tend to aggregate one another and adhere on the surface of balls even in organic solvents. Thus, improvement of the milling conditions is necessary in order to obtain the high performance $Sm_2Fe_{17}N_x$ powder.

In this chapter, a new grinding procedure based on ball milling in organic solution containing a surfactant is applied to prepare the powder samples of $Sm_2Fe_{17}N_x$.

2.2. Experimental Details

The $Sm_2Fe_{17}N_x$ powder was prepared by heating the powder of Sm_2Fe_{17} in an NH_3-H_2 atmosphere according to the procedure described elsewhere[11]. After the annealing at 723 K for a few hours in

Ar, the resulting raw powder with particle size = 50 - 100 μm was ground by ball milling in n-hexane solution containing Aerosol OT (di-2-ethylhexyl sodium sulfosuccinate, $C_{20}H_{37}O_4SO_3Na$) using a glass pot and steel balls. The n-hexane used here was distilled in the presence of Na metal to remove water residue completely and all the manipulations were carried out in a purified Ar or N_2 atmosphere. The samples were identified on the basis of x-ray diffraction (XRD) patterns measured using a CuK_α radiation, and nitrogen and oxygen contents were checked on a nitrogen and oxygen analyzer (Horiba, EMGA-550). The measurement of sodium content was performed on inductively coupled plasma atomic emission spectroscopy apparatus (Shimadzu, ICPS-1000IV). The relative surface area of the samples were measured by BET method. Magnetization hysteresis curves of the powder samples were measured on a vibrating sample magnetometer (Toei, VSM-5-15) in a range of magnetic field up to ±1.2 MAm^{-1} at room temperature after a magnetization at 4.8 MAm^{-1} by a pulsed field generator.

2.3. Results and Discussion

The ball milling technique performed in the presence of a solvent produces fine powder materials without inducing any extra strain during the grinding process, but the powder of $Sm_2Fe_{17}N_x$ tended to aggregate one another and to adhere to steel balls during milling in pure n-hexane, and it was difficult to collect the ground powder. On the other hand, it was found that the ball milling in the n-hexane solution containing a surfactant, Aerosol OT, was a good procedure to grind the raw $Sm_2Fe_{17}N_x$ efficiently. Particle shape and size of the ground powder samples of $Sm_2Fe_{17}N_x$ were shown in Fig. 2.1 and magnetization hysteresis curves for the powder samples are shown in Fig. 2.2. In addition, the fundamental magnetic data and oxygen contents are listed in Table 2.1. Although the powder ground for 72 h in pure n-hexane (Fig. 2.1(a)) and for 18 h in the n-hexane solution containing 5 wt% of Aerosol OT against the raw powder (Fig. 2.1(b)) had similar mean particle size each other, the B_r and H_{cj} values and the oxygen content of them were quite different. The B_r and H_{cj} values and the oxygen content of the former were respectively 1.00 T, 0.63 Am^{-1} and 0.81 wt%, but the values were improved for the latter as 1.36 T, 1.08 MAm^{-1} and 0.59 wt%, respectively. Moreover, the specific surface area of the former (1.6 m^2g^{-1}) was much larger than that of the latter (0.24 m^2g^{-1}). It was found by the magnified SEM photographs (Fig. 2.3) that the surface of the latter was smoother than that of the former. These
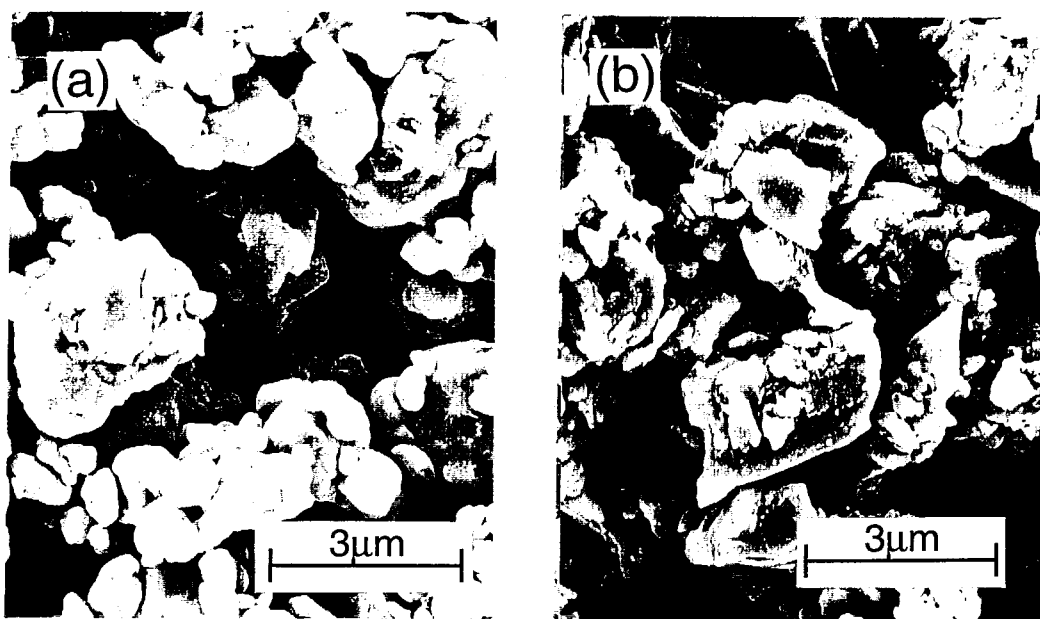
22

Figure 2.1. SEM micrographs of the powder samples of $Sm_2Fe_{17}N_x$ prepared by ball milling in n-hexane solution (a) without the surfactant for 72 h and (b) with it for 18 h.
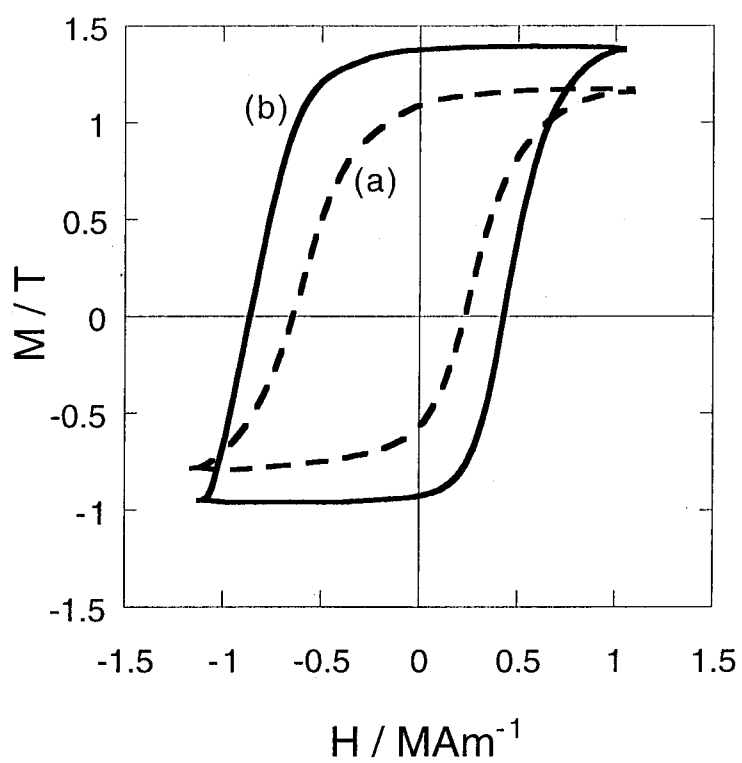

Figure 2.2. Magnetic hysteresis curves of the powder samples as shown in Fig. 2.1.

are indicated that there is no extra friction during the milling owing to addition of the surfactant. The surfactant seems to have some effects on prevention of aggregation for the ground $Sm_2Fe_{17}N_x$ particles by formation of reversed micelles around them and reduction of mechanical strength of them (Rehbinder effect). Hence, for the $Sm_2Fe_{17}N_x$ powder ground in the solution with the surfactant, the B_r value was maintained at high level because of small content of oxygen by short milling time, and the high H_{cj} value was achieved since small amounts of nucleation points exists on the smooth surface of the

Table 2.1. Fundamental magnetic data and oxygen contents of the $Sm_2Fe_{17}N_x$ powder ground under various conditions.

Surfactant[a] (wt%)	Milling time (h)	Oxygen content (wt%)	Magnetic properties			Specific surface area (m^{2}g^{-1})
			M_s (T)	B_r (T)	H_{cj} (MAm^{-1})	
0	72	0.81	1.18	1.00	0.63	1.60
5	18	0.59	1.39	1.37	0.86	0.24
5	72	0.99	1.32	1.28	1.13	0.66

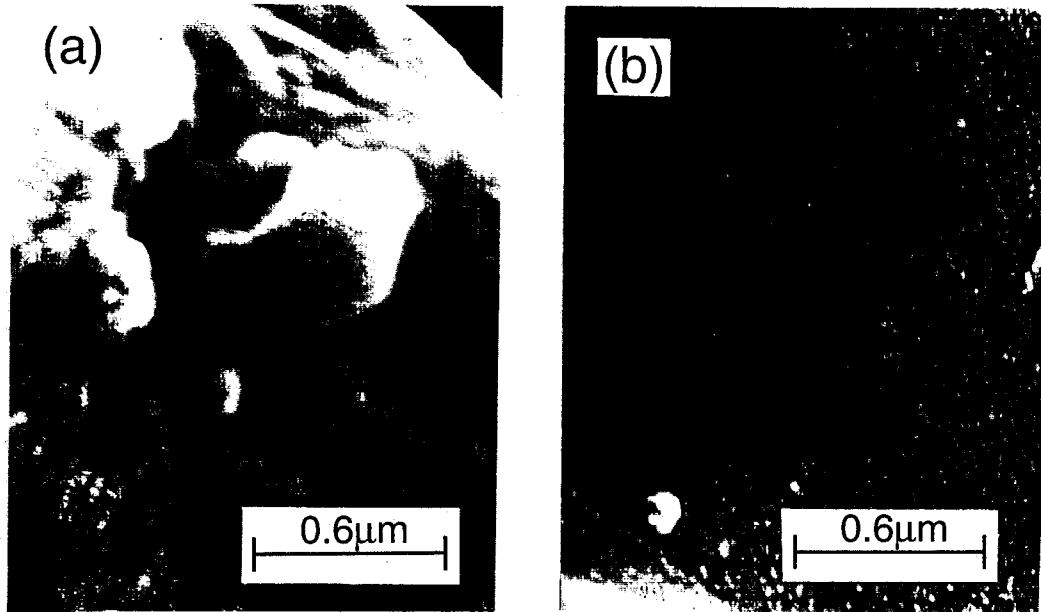[a]Aerosol OT ($C_{20}H_{37}O_4SO_3^-Na^+$)

Figure 2.3. Magnified SEM micrographs of the powder samples as shown in Fig. 2.1.

particles.

Figures 2.4(b) and 2.4(c) show the XRD patterns for the powder samples of $Sm_2Fe_{17}N_x$ ground by ball milling for 24 and 72 h in n-hexane solution containing the surfactant, while Fig. 2.4(a) shows that for the raw powder sample. The raw powder sample exhibited an XRD pattern which was completely assignable to the rhombohedral symmetry of space group R-3m as reported elsewhere[28]. No significant
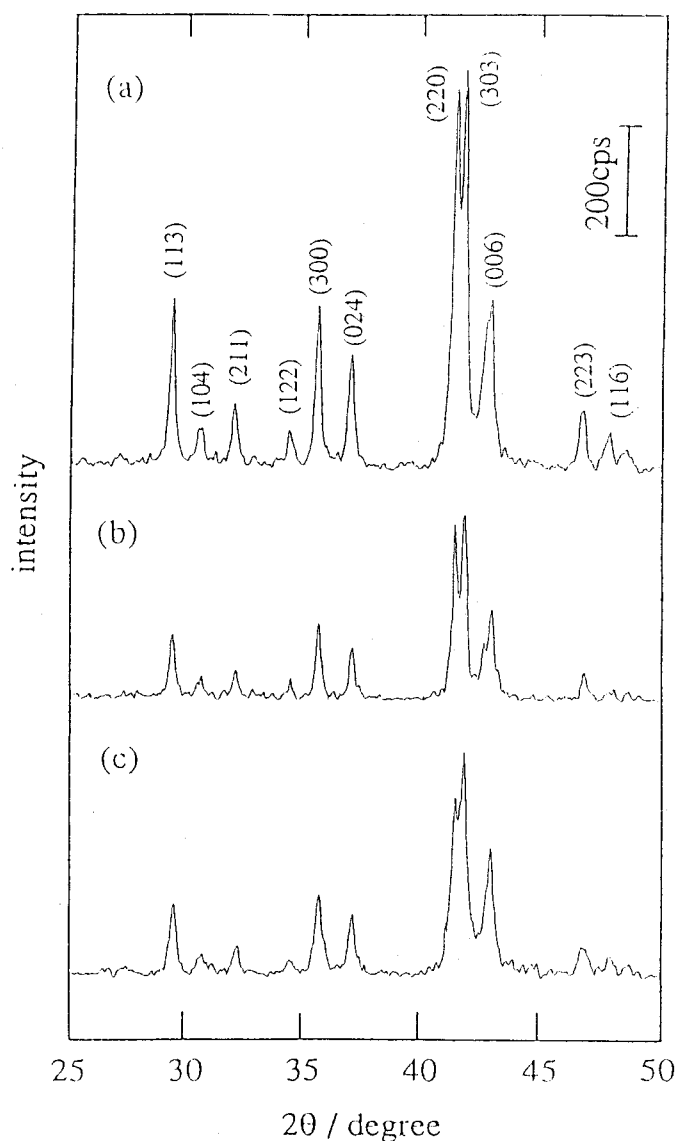

Figure 2.4. XRD patterns of $Sm_2Fe_{17}N_x$ powder (a) before fine grinding (particle size = 50-100μm), (b) ground for 24 h, and (c) ground for 72 h, in n-hexane solution containing the surfactant (5 wt%).

peak representing the decomposition fractions such as SmN and α-Fe was observed on the XRD patterns even after the ball milling for 24 or 72 h. Therefore, it is concluded that marked oxidation hardly occurs on the surface of the resultant powder sample, which was also supported by the analytical data of the oxygen content. However, the peak intensity in the diffraction pattern of the powder samples prepared by the ball milling gradually decreased with grinding time.

Figure 2.5 shows the milling time dependence of the B_r, H_{cj} and BH_{max} values of the $Sm_2Fe_{17}N_x$ powder ground in the n-hexane solution containing the surfactant (5 wt% for $Sm_2Fe_{17}N_x$ powder). The H_{cj} value increased as the milling time got longer. In particular, the drastic increase of the H_{cj} values was observed on the powder milled within 12 h. Mean particle size of the powder milled for 12 h was evaluated at around 3 µm, which corresponds the single domain size[29], by SEM observation.
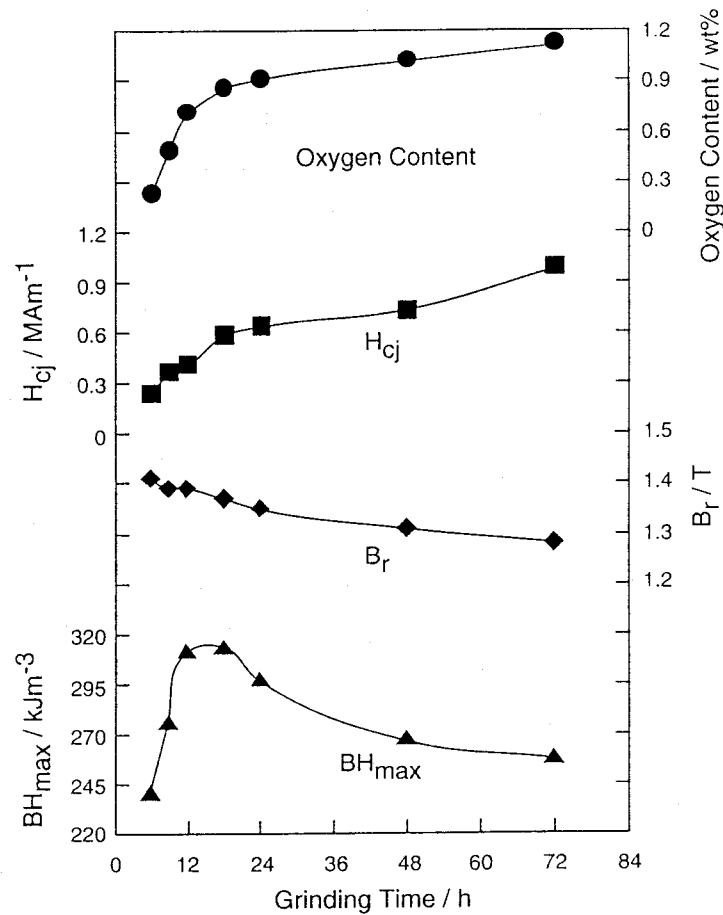

Figure 2.5. Milling time dependence for the oxygen contents and magnetic properties of $Sm_2Fe_{17}N_x$.

On the contrary, the B_r value decreased with long milling time. The specific surface area expands with a decrease in the particle size and the powder gets easy to be oxidized. The oxygen content of the ground $Sm_2Fe_{17}N_x$ powder increased certainly with the increase in the milling time, hence the B_r value was reduced because of formation of non-magnetic amorphous oxide[30]. The dependence of B_r and H_{cj} value on the milling time were contrary to each other, so that it is necessary for getting the powder with high BH_{max} value that the powder is attended with well-balanced B_r and H_{cj} values. The highest BH_{max} value (313 kJm-3) was achieved by milling for 18 h.

As the amount of the added surfactant against the raw powder increased, the milling time needed to achieve the highest BH_{max} value got shorter but there was not effect any more when more than 15 wt% of the surfactant added. The rectangularity improved with the increase in the amount of the solution. Since the time for ground $Sm_2Fe_{17}N_x$ powder dispersing into a large amount of the solution is long compared with a case of milling in a small amount of the soltion, the $Sm_2Fe_{17}N_x$ powder is ground uniformly and the particle size are narrowly distributed. Optimum parameters for milling time, amounts of surfactant, solvent and steel balls resulted in a BH_{max} value of up to 330 kJm-3.

Tajima et al. have reported that alkali or alkaline earth ion-free surfactant should be used in a ball milling of $Sm_2Fe_{17}N_x$ powder in organic solutions because the ions are impurity[31]. However, the sodium ion based on residue of the surfactant was not detected on the powder samples by the atomic emission spectroscopy. The very popular surfactant containing alkali or alkaline earth element are therefore able to be used for the ball milling of $Sm_2Fe_{17}N_x$ powder in n-hexane solution.

2.4. Conclusions

Ball milling in an organic solution containing the surfactant (Aerosol OT) should is a suitable procedure for obtaining the $Sm_2Fe_{17}N_x$ powder with a fine and uniform particle size as well as smooth surface, since addition of the surfactant have some effects on suppression of the powder samples from aggregation to each other, adhesion onto the surface of steel balls and introduction of distortion into the particles. In addition, the oxidation of $Sm_2Fe_{17}N_x$ powder during milling hardly occurred and the amount of strain induced in the particles is relatively small because of short milling time, and the magnetic properties of the $Sm_2Fe_{17}N_x$ powder obtained here are considerably enhanced compared

27

with the one obtained by milling without the surfactant.

Chapter 3

Improvement of Resistivity against Oxidation for $Sm_2Fe_{17}N_x$ Fine Powder with Zinc Metal Coating Produced by Photoinduced Decomposition of $Zn(C_2H_5)_2$

3.1. Introduction

Although the oxidation of $Sm_2Fe_{17}N_x$ powder during milling is able to be suppressed by improvement of the milling conditions and the $Sm_2Fe_{17}N_x$ fine powder with excellent magnetic properties can be obtained in Chapter 2, the resulting powder tends to be oxidized due to its high reactivity. Hence, the surface of powder must be protected from oxidation by some way. Otani et al.[20] have reported that zinc bonded $Sm_2Fe_{17}N_x$ magnets have a high H_{cj} value. Zinc metal can neutralize nucleation points by smoothing the surface of particles and removing the soft magnetic phase as a paramagnetic phase such as Zn_7Fe_3[20] or $Sm_2(Fe,Zn)_{17}N_x$[32]. It is possible therefore that the zinc coating on the surface of $Sm_2Fe_{17}N_x$ fine powder improve not only resistivity against oxidation but the coercivity.

The surface of the powder particles is stabilized by coating with zinc metal produced by the photodecomposition of diethylzinc $(Zn(C_2H_5)_2)$ in this chapter. Furthermore, their magnetic characteristics are investigated from the viewpoint of the practical use as permanent magnet materials.

3.2. Experimental Details

The $Sm_2Fe_{17}N_x$ fine powder was prepared by the procedure described in Chapter 2 and the platy sample of the $Sm_2Fe_{17}N_x$ was obtained by means of the plasma method in an N_2-H_2 mixed gas[11]. Zinc coating was performed by two different procedures, i.e. CSD (Chemical Solution Deposition) and CVD (Chemical Vapor Deposition) methods (see Fig. 3.1). For the CSD method, the powder (6 g) or platy samples ($10 \times 5 \times 3$ mm) were put into a quartz cell and added 20 cm^3 of n-hexane solution containing 13.1 mol% $Zn(C_2H_5)_2$. For the CVD method, the $Sm_2Fe_{17}N_x$ powder (6 g) or plates ($10 \times 5 \times 3$ mm) were put on a glass filter of a glass cell while an n-hexane solution containing $Zn(C_2H_5)_2$

(a)

Zn(C₂H₅)₂/*n*-hexane

Sm₂Fe₁₇Nₓ fine powder

quartz window

UV light

(b)

UV light

quartz window

He gas
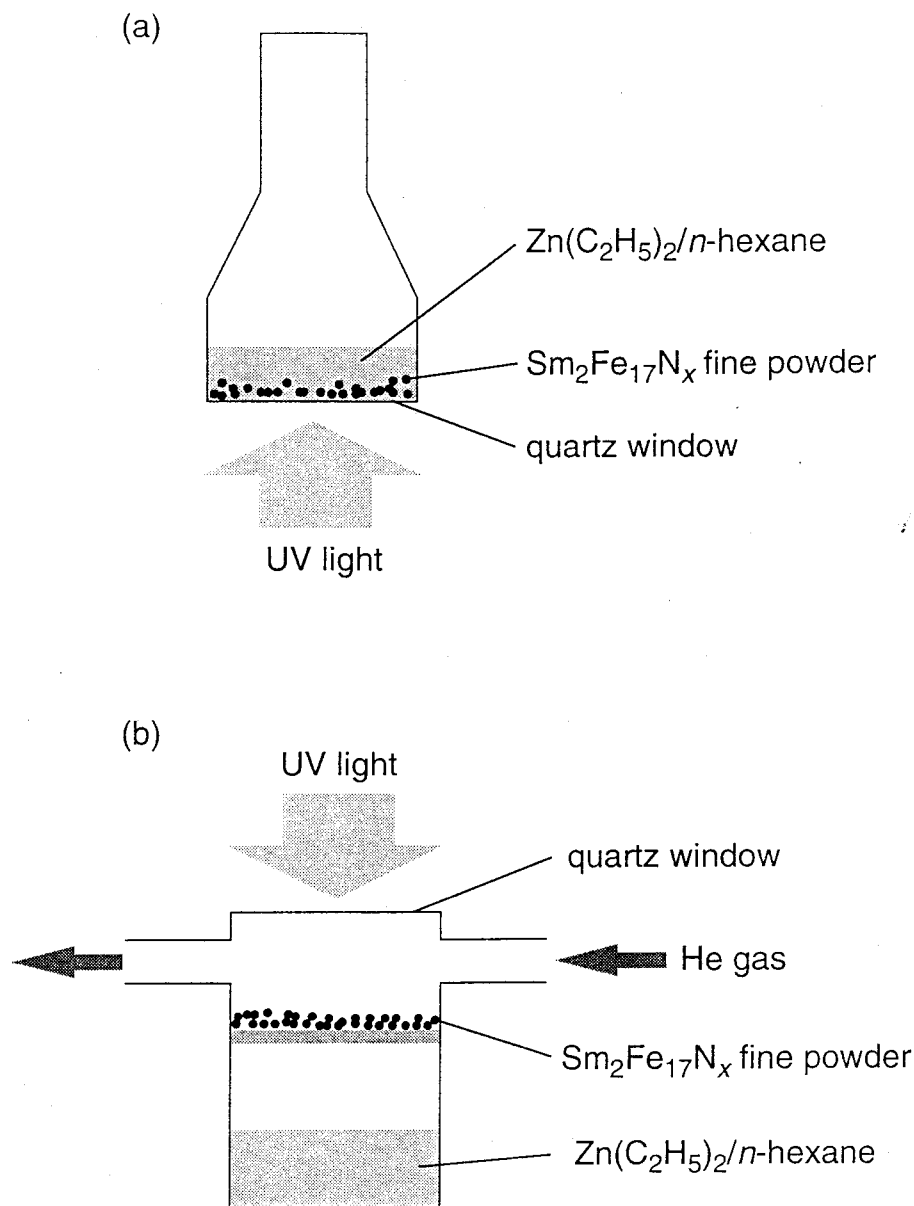
Sm₂Fe₁₇Nₓ fine powder

Zn(C₂H₅)₂/*n*-hexane

Figure 3.1. Glass cells for the photoinduced zinc metal coating by (a) CSD and (b) CVD methods.

was introduced in a lower part of the cell. Decomposition of $Zn(C_2H_5)_2$ was carried out by irradiation of ultraviolet rays for several hours using a low pressure mercury arc. The powder samples were washed with the distilled *n*-hexane and dried. Compression bonded magnets were made by mixing the resulting powder with 2.5 wt% of an epoxy resin, molding under pressure of 1.4 GPa in a magnetic field of 1.4 MAm⁻¹, and heating for cure at 353 K for 4 h. The samples were identified on the basis of x-ray diffraction (XRD) patterns measured using a CuK_α radiation, and nitrogen and oxygen contents

were checked on a nitrogen and oxygen analyzer (Horiba, EMGA-550). The measurement of zinc content was performed on inductively coupled plasma atomic emission spectroscopy apparatus (Shimadzu, ICPS1000IV). Magnetization hysteresis curves of the powder and bonded samples were measured on a vibrating sample magnetometer (Toei, VSM-5-15 and Riken Denshi, BHV-510) in a range of magnetic field up to ± 1.2 MAm^{-1} at room temperature after a magnetization at 4.8 MAm^{-1} by a pulsed field generator.

3.3. Results and Discussion

3.3.1. Zinc Coating of Sm$_2$Fe$_{17}$N$_x$ Powder

Diethylzinc has a UV-visible absorption spectrum with a strong peak at 248 nm. The photodecomposition occurs under irradiation with UV light as shown in Eq. (3.1):

$$Zn(C_2H_5)_2 \xrightarrow{h\nu} Zn + C_mH_n \ (C_2H_4, C_2H_6, C_4H_8 \ or \ C_4H_{10}) \qquad (3.1)$$

This reaction scheme suggests that the resulting hydrocarbons (C_mH_n) are too inert to decompose or contaminate the Sm$_2$Fe$_{17}$N$_x$ fine powder, so that the intrinsic magnetic properties of Sm$_2$Fe$_{17}$N$_x$ should be observable and potentially useful in application.

The SEM photographs of the platy samples of Sm$_2$Fe$_{17}$N$_x$ with zinc coating (Zn/Sm$_2$Fe$_{17}$N$_x$) produced by the CSD and CVD methods are shown in Fig. 3.2. Both of the surfaces of the Zn/Sm$_2$Fe$_{17}$N$_x$ samples were covered with zinc detected by fluorescent x-rays analysis measurements on a micron scale. The CSD sample had rough surface with some cracks, while the surface of the CVD sample was uniformly covered by a number of small particles. Figure 3.3 shows the AES profiles of the CSD and CVD samples before and after etching for 5 nm (conversion to SiO$_2$). The AES profile of the CSD sample before etching was dominated by the Zn LMM signal with peaks which were assigned to ZnO (499.0 eV). The shoulder peaks at 494.5 and 491.0 eV assigned to Zn LMM signal for zinc metal appeared after the etching. On the other hand, the AES profile of the as-prepared CVD sample consisted from the peaks assigned to zinc metal and ZnO. The peaks assigned to zinc metal were considerably
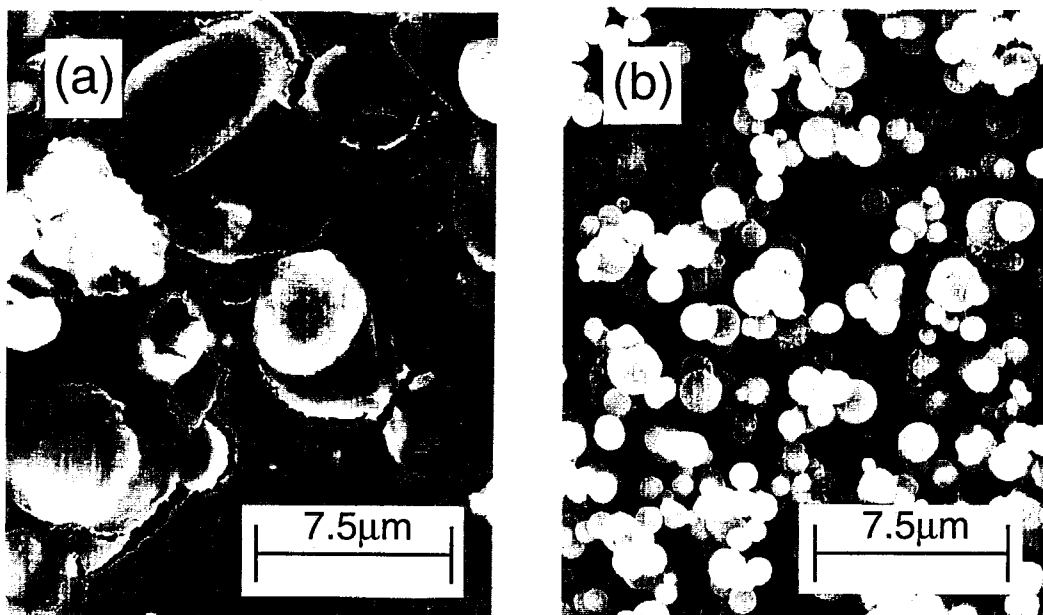
Figure 3.2. SEM micrographs for the plate samples of $Sm_2Fe_{17}N_x$ with zinc coating by (a) CSD method and (b) CVD method.

Binding Energy / eV
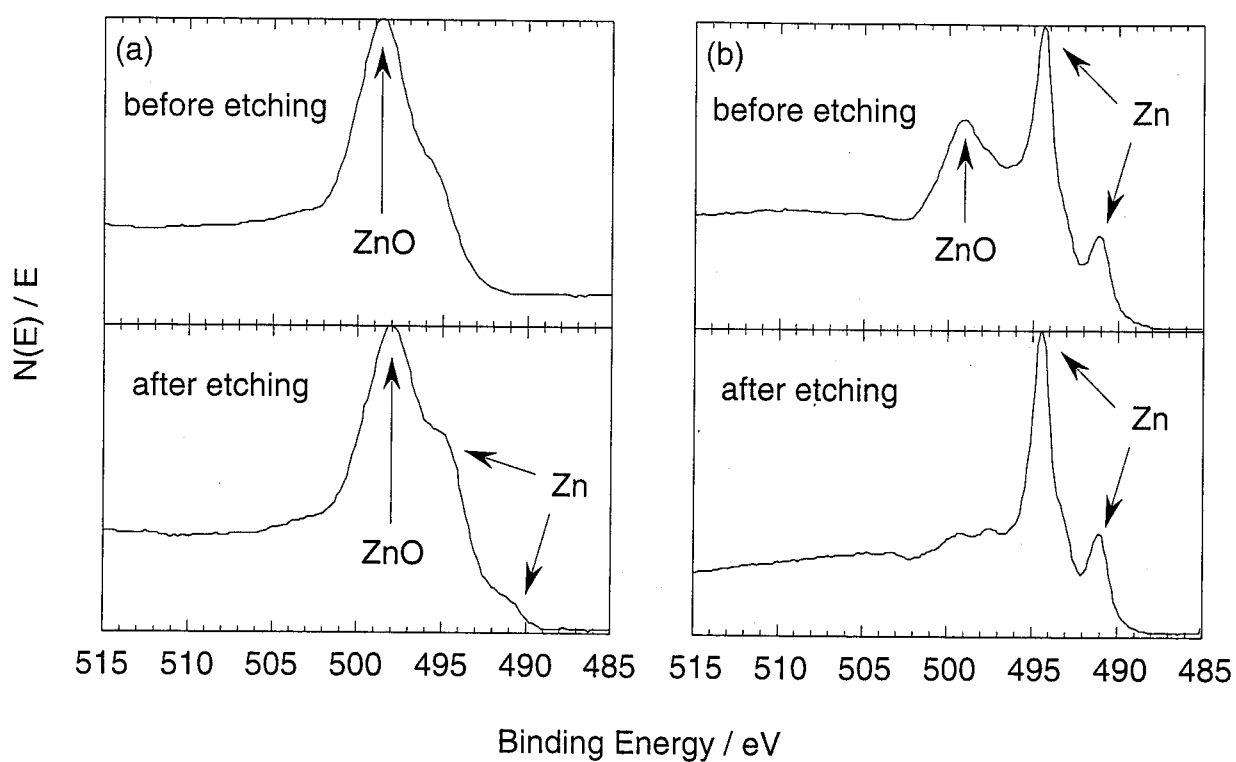
Figure 3.3. AES patterns for the plate samples of $Sm_2Fe_{17}N_x$ with zinc coating by (a) CSD method and (b) CVD method.

32

sharpened, and the peak for ZnO almost disappeared after the etching. In addition, the ratio of the peak areas for O 1s signals against Zn 2p signals for the CSD sample before and after the etching were respectively 0.72 and 0.67, the ratio for the CVD sample decreased from 0.69 to 0.24 through the etching. These results suggest that $Zn(C_2H_5)_2$ decomposed to zinc metal on the surface of $Sm_2Fe_{17}N_x$ plate, and the surface of zinc coating was oxidized during handling. Furthermore, the zinc coating obtained by the CVD procedure is expected to provide good oxidation resistance compared with the CSD one.

The oxygen content and the fundamental magnetic data of the $Sm_2Fe_{17}N_x$ powder sample with and without the zinc coating are listed in Table 3.1. The B_r values for $Zn/Sm_2Fe_{17}N_x$ samples did not

Table 3.1. Magnetic properties and oxygen contents of $Sm_2Fe_{17}N_x$ powder without and with zinc coating.

| Zinc coating	Heat treatment		Oxygen content (wt%)	Magnetic properties		
	Temperature (K)	Time (h)		H_{cj} (MAm^{-1})	B_r (T)	BH_{max} (kJm^{-3})
none	none	none	0.59	0.86	1.37	313
none	423	1	0.88	0.84	1.12	182
none	423	10	1.06	0.40	0.75	69
CSD	none	none	0.56	0.84	1.35	300
CSD	423	1	0.54	0.82	1.35	295
CSD	423	10	0.55	0.76	1.38	309
CSD	523	1	0.57	0.62	1.26	236
CSD	623	1	0.53	0.57	0.83	95
CSD	723	1	0.55	0.60	0.78	88
CVD	none	none	0.43	0.68	1.31	286
CVD	423	1	0.58	0.69	1.30	272
CVD	423	10	0.57	0.68	1.25	258
CVD	523	1	0.38	0.62	1.33	292
CVD	623	1	0.46	0.42	1.13	192
CVD	723	1	0.52	0.42	0.80	102
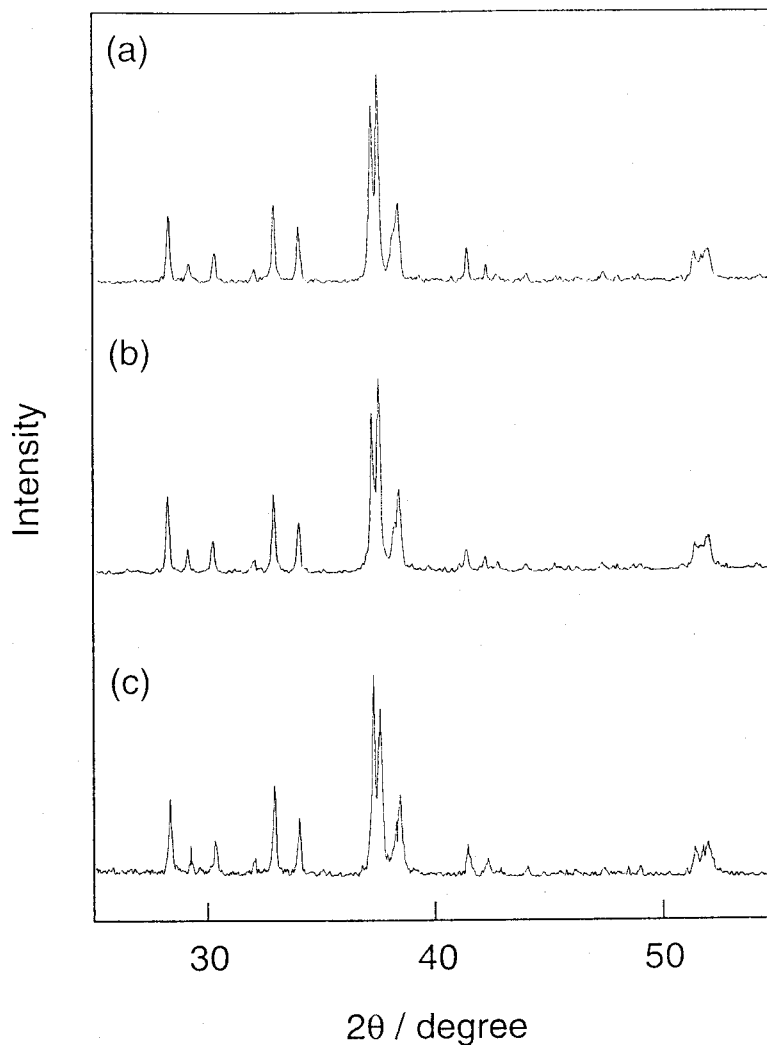
Figure 3.4. XRD patterns for the $Sm_2Fe_{17}N_x$ powder (a) without zinc coating, (b) with zinc coating by CSD method and (c) with zinc coating by CVD method.

change very much compared with the $Sm_2Fe_{17}N_x$ powder due to the small amount of non-magnetic zinc (< 1 wt%). The XRD patterns of them were similar to one another (see Fig. 3.4), and there was no extra peak for the $Zn/Sm_2Fe_{17}N_x$ powder, such as α-Fe or Zn-Fe intermetallic compounds, except the peaks assigned to $Sm_2Fe_{17}N_x$. Although it has been reported that zinc metal can enhance the H_{cj} value of the $Sm_2Fe_{17}N_x$ owing to removing nucleation points[17], the H_{cj} values of the $Zn/Sm_2Fe_{17}N_x$ samples also did not change very much. These results can mean that the zinc obtained here only coats over the particle surface and did not form any Zn-Fe compounds which enhance the H_{cj} values.

The heat treatment time dependence of fundamental magnetic properties and oxygen contents of the $Sm_2Fe_{17}N_x$ and $Zn/Sm_2Fe_{17}N_x$ powder are shown in Fig. 3.5. For the $Sm_2Fe_{17}N_x$ powder, the B_r and H_{cj} values decreased markedly and oxygen content increased through the heat treatment at 423 K. On the other hand, the oxygen contents for the $Zn/Sm_2Fe_{17}N_x$ powder prepared by both the CSD and
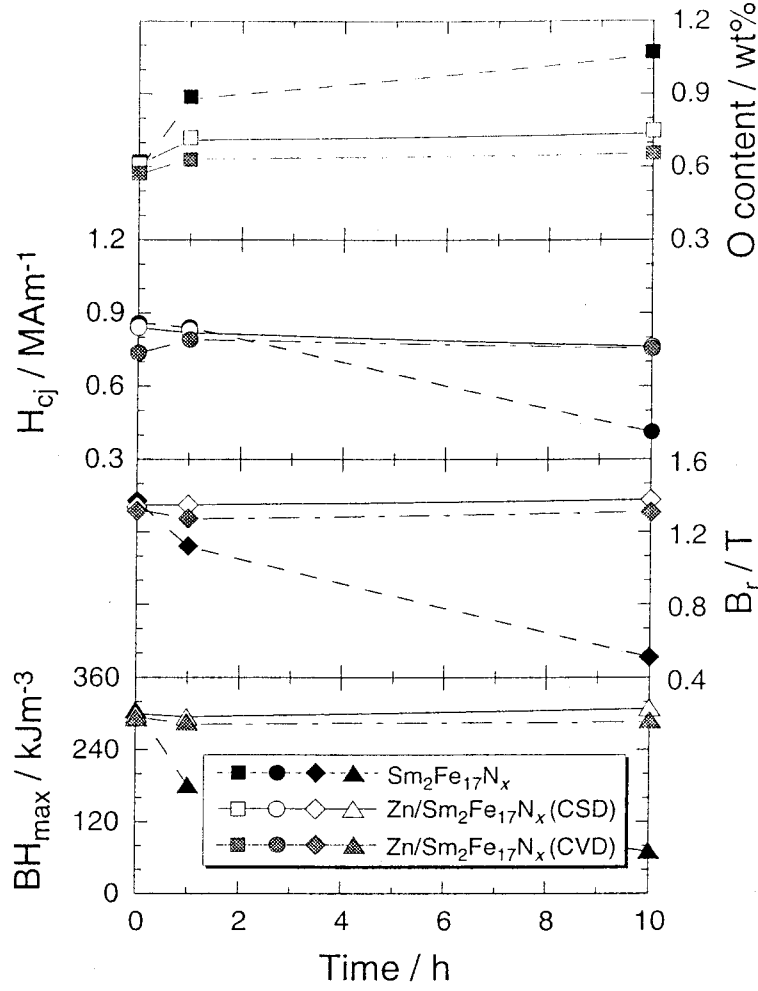
34

Figure 3.5. Heat treatment time dependence of oxygen contents and fundamental magnetic values of the $Sm_2Fe_{17}N_x$ powder without and with zinc coating (in Ar, at 423 K).

CVD methods increased a little through the heat treatment at the same temperature, which was enough for generating the bonded magnets, and the fundamental magnetic values were retained at high levels. This can be explained as the zinc coatings prevented the $Sm_2Fe_{17}N_x$ powder from decomposition *via* oxidation. When the heat treatment temperature raised from 423 K, the B_r and H_{cj} values for the CSD powder decreased, but there was little change in the oxygen contents and XRD patterns through the heat treatment. The zinc coating obtained by the CSD method consisted of the mixture of zinc metal and zinc oxide, hence it suggests that the oxygen in the zinc coating migrates to the inner $Sm_2Fe_{17}N_x$ and the nitride partly decomposes to amorphous-like oxide. The H_{cj} value after heat treatment at 723 K might be recovered because of formation of non-magnetic Zn-Fe intermetallic compounds on the

surface, but we cannot confirm it. Since the surface of the $Sm_2Fe_{17}N_x$ powder cannot be covered uniformly for the CVD method because the decomposition of $Zn(C_2H_5)_2$ vapor does not take place on the shadow area of surface, oxidation might occur at the uncoated area. This is indicated by the oxygen contents of the powder samples. Therefore, if the whole surface of $Sm_2Fe_{17}N_x$ powder can be completely coated with zinc using the CVD method, the oxidation resistance of the $Sm_2Fe_{17}N_x$ fine powder is expected to be improved considerably.

3.3.2. Magnetic Properties of Bonded Magnets

The demagnetization curves for the $Zn/Sm_2Fe_{17}N_x$ powder prepared by CSD method and its bonded magnet were shown in Fig. 3.6. It can be judged that the $Zn/Sm_2Fe_{17}N_x$ powder was not damaged seriously by some processes to produce the bonded magnets because the B_r value of the bonded magnet agreed with the values calculated by taking account of the density reduction due to bonding. However, the H_{cj} value decreased after bonding owing to chipping the corners of molding
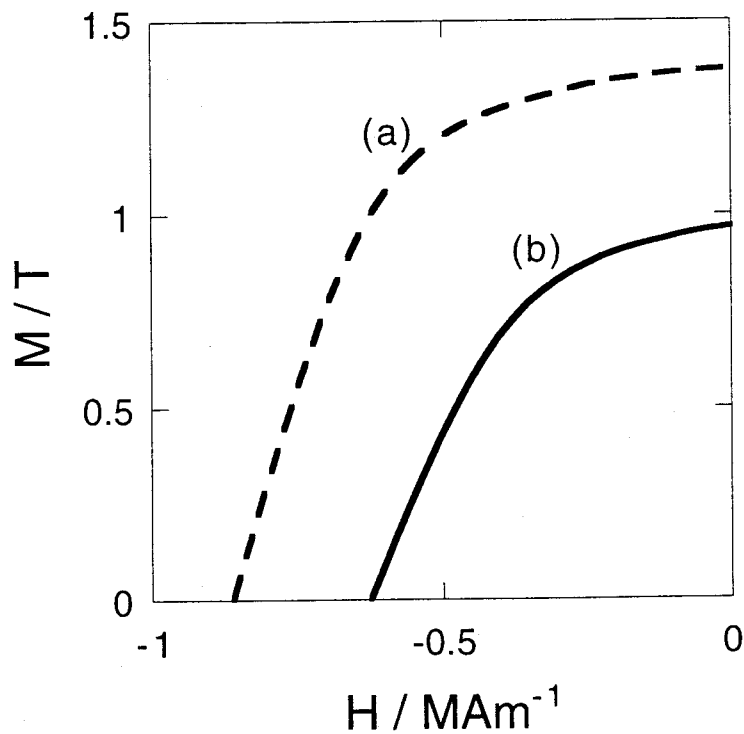

Figure 3.6. Demagnetization curves for (a) starting powder and (b) bonded magnet of $Zn/Sm_2Fe_{17}N_x$

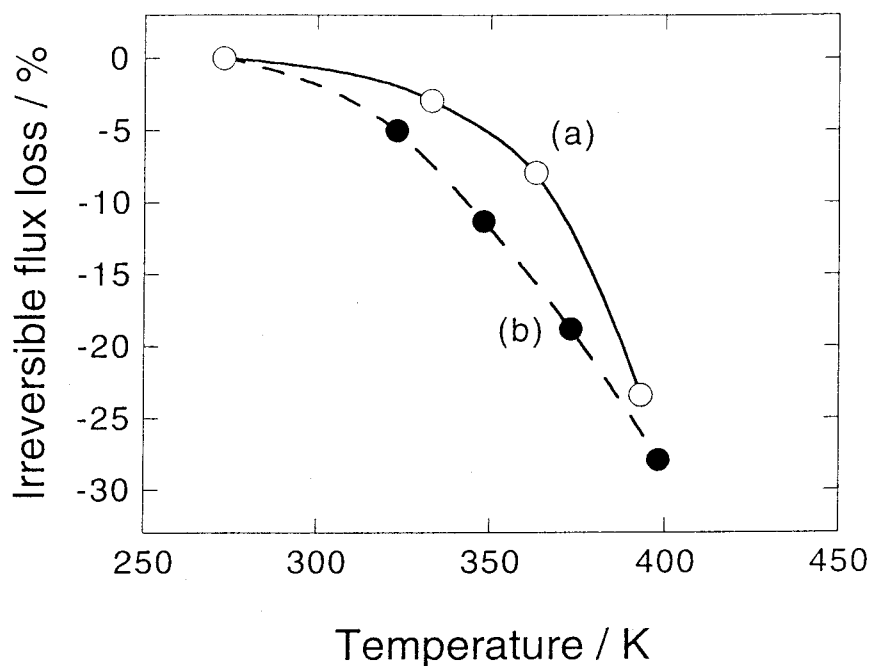**Figure 3.7.** Irreversible flux loss curves of the bonded magnets of (a) $Zn/Sm_2Fe_{17}N_x$ and (b) $Sm_2Fe_{17}N_x$ (ref. 33).

during handling, and the rectangularity of the resulting bonded magnet was lowered compared with that of the raw powder for orientation of the particles was disordered during pressing. Nevertheless, the BH_{max} value of the bonded magnet made by using the CSD powder attained the highest value (176 kJm^{-3}) among those as reported to date, $e.g.$ 164 kJm^{-3}[33].

Figure 3.7 shows the irreversible flux loss curve of the $Zn/Sm_2Fe_{17}N_x$ (CSD) bonded magnet, together with that of uncoated $Sm_2Fe_{17}N_x$ one. Iriyama et al. have reported that the irreversible flux loss of an uncoated $Sm_2Fe_{17}N_x$ magnet after heat treatment at 323 K in air is 5%[34]. After heat treatment at temperatures above 348 K, however, the irreversible flux loss was considerably increased due to the extensive oxidation of the $Sm_2Fe_{17}N_x$ powder. On the other hand, the irreversible flux loss of $Zn/Sm_2Fe_{17}N_x$ magnet is small (about 7 %) even after heat treatment at 363 K. This is attributed to the good oxidation resistance of the $Zn/Sm_2Fe_{17}N_x$ raw powder, which enables it to be used at high temperature compared with the $Sm_2Fe_{17}N_x$ bonded magnet.

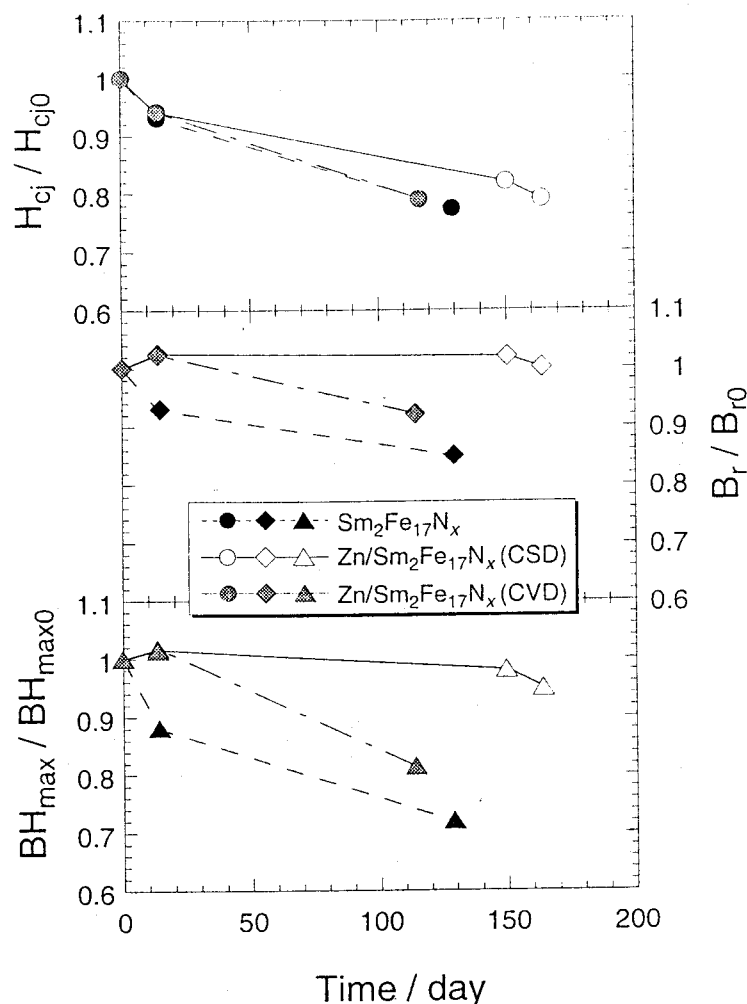**Figure 3.8.** Exposure time dependence of fundamental magnetic values of the $Sm_2Fe_{17}N_x$ bonded magnets without and with zinc coating (in air, at room temperature).

After exposure to air at room temperature for 15 days, the BH_{max} value for the uncoated $Sm_2Fe_{17}N_x$ bonded magnet decreased below 90% of the initial value (see Fig. 3.8). Contrary, for the $Zn/Sm_2Fe_{17}N_x$ (CSD) bonded magnet, the value was retained even after 150 days. It can be concluded therefore that the resulting $Zn/Sm_2Fe_{17}N_x$ bonded magnet represents a great advance in the practical use of uncoated $Sm_2Fe_{17}N_x$-based magnets.

3.4. Conclusions

The magnetic properties of $Sm_2Fe_{17}N_x$ powder are not changed very much after the coating with zinc produced by the photodecomposition of $Zn(C_2H_5)_2$ because the amount of non-magnetic zinc is

quite low. However, the oxidation resistance of $Sm_2Fe_{17}N_x$ fine powder is effectively improved by this coating. Furthermore, the bonded $Zn/Sm_2Fe_{17}N_x$ magnets have the highest BH_{max} value reported to date, and the BH_{max} value is retained even after exposure against air for 150 days.

Chapter 4

Improvement of Magnetic Properties of $Sm_2Fe_{17}C_x$ by Substitution of Co for Fe as Material for Sintered Magnets

4.1. Introduction

Although the nitrides and carbonitrides, $Sm_2Fe_{17}X_x$ or $Nd(Fe,M)_{12}X_x$ (X = C and/or N) have excellent magnetic properties as permanent magnets, their thermostability is not enough to give sintered magnets. Buschow et al.[35,36] have shown that the introduction of carbon atoms by means of cast method into the R_2Fe_{17} crystal lattice leads to elevation of the T_c value and to change of the easy magnetization direction (EMD) from the basal plane to the c-axis for R = Sm. Moreover, the $Sm_2Fe_{17}C_x$ compound with $x < 1$ is stable state, so that it can be sintered at high temperature without decomposition. However, the T_c and coercivity are considerably poor for use as permanent magnet material. On the other hand, it is well known that the partial substitution of Co for Fe in Sm_2Fe_{17} also leads to elevation of T_c value and uniaxial anisotropy. This chapter describes that the composition dependence on the magnetic anisotropy and the thermal stability of $Sm_2(Fe_{1-x}Co_x)_{17}C_y$ with a view to producing a high performance sintered permanent magnet.

4.2. Experimental Details

Samples of $Sm_2(Fe_{1-x}Co_x)_{17}C_y$ were prepared by arc melting of starting materials, Sm, Fe, Co metal and C, followed by annealing on a Ta boat in an Ar atmosphere (99.999%) at 1373 K for 48 h. A 10 mol% excess amount of Sm metal was added to the stoichiometric mixture in order to compensate for the evaporation loss of the Sm component during the melting and annealing processes. The samples were identified on the basis of x-ray diffraction (XRD) measurements, compositions of Sm, Fe and Co were determined by means of inductively coupled plasma atomic emission spectroscopy (Shimadzu, ICPS-1000IV), and carbon content was determined by use of a carbon analyzer (Kokusaidenki, COULOMATIC-C). The EMD of the samples was elucidated from the XRD patterns of the magnetically

aligned samples in a magnetic field of 720 kAm-1 at 350 K. Their T_c values were evaluated from the temperature dependence curves of magnetization, which were measured by means of a magnetic balance (Shimadzu, MB-11) in a magnetic field of 13.4 kAm-1 and a temperature range from 300 to 1000 K.

4.3. Results and Discussion

Figure 4.1 shows the XRD patterns of $Sm_2(Fe_{1-x}Co_x)_{17}C_y$ with various x and y values, and their lattice parameters are listed in Table 4.1. The XRD patterns observed on all the $Sm_2(Fe_{1-x}Co_x)_{17}C_y$ compounds were completely assigned on the basis of the Th_2Zn_{17}-type crystal lattice. The lattice parameters were in good agreement with the reported values. The unit cell volume decreased with the concentration of Co but increased with the carbon content[37,38]. This indicates that carbon atoms share the interstitial 9e sites in the rhombohedral symmetry (space group = R-3m).

The magnetization in the field of 720 kAm-1 at 300 K and the T_c value of the $Sm_2(Fe_{1-x}Co_x)_{17}C_y$ are listed in Table 4.1. The magnetization value increased with increase of Co content up to $x = 0.3$, but decreased at $x = 0.5$. According to the Slater-Pauling curve, the magnetic moments of a series of $Fe_{1-x}Co_x$ alloys produce a maximum around $x = 0.3$. Therefore, it is reasonable that a maximum is also

Table 4.1. Cobalt content, x, carbon content, y, lattice parameters, a and c, unit cell volume, V, magnetization, M, and Curie temperature, T_c, for $Sm_2(Fe_{1-x}Co_x)_{17}C_y$.

Composition		Lattice parameters (Å)		V (Å³)	M (T)[a]	T_c (K)
x	y	a	c			
0.0	0.0	8.56	12.43	789	1.14	390
0.1	0.1	8.56	12.47	791	1.29	590
0.1	0.3	8.58	12.46	794	1.34	610
0.3	0.1	8.54	12.49	789	1.46	810
0.3	0.3	8.55	12.47	790	1.57	850
0.0	0.5	8.64	12.54	810	1.32	490
0.5	0.0	8.46	12.40	767	1.43	>1000

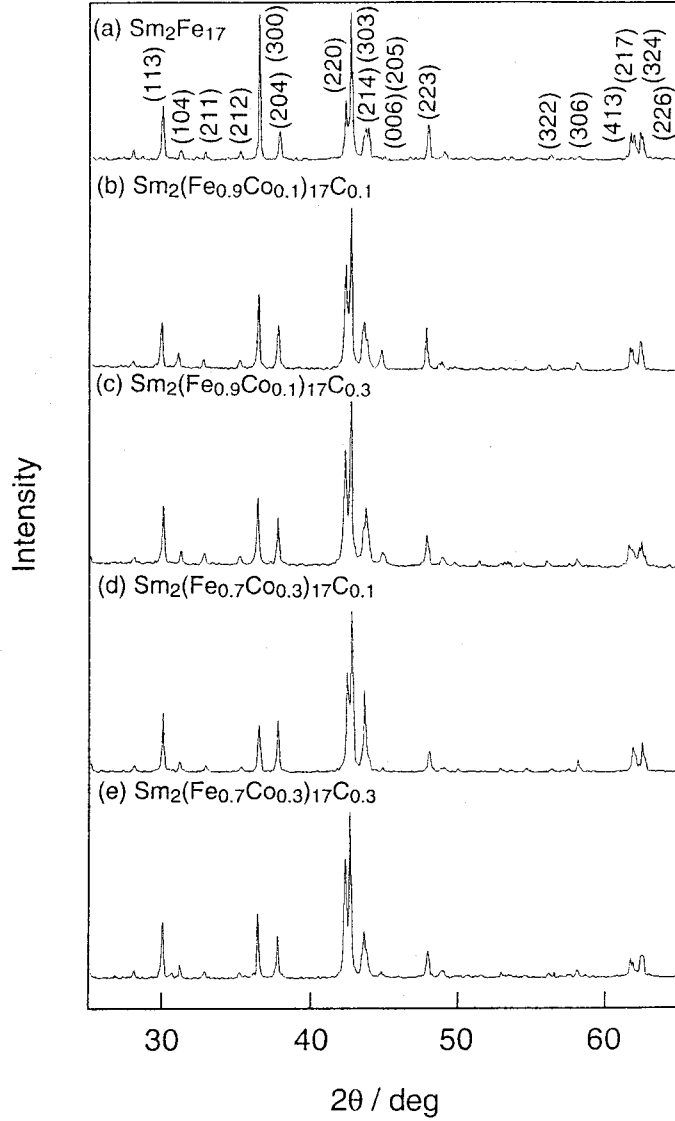[a]Magnetization value in the field of 720 kAm-1 at 300 K.

41

Figure 4.1. XRD patterns of the $Sm_2(Fe_{1-x}Co_x)_{17}C_x$ samples.

observed for the $Sm_2(Fe_{1-x}Co_x)_{17}C_y$ compound around $x = 0.3$. The magnetization of $Sm_2(Fe_{1-x}Co_x)_{17}C_y$ is also effectively elevated with increase of carbon content as well as $Sm_2Fe_{17}C_x$. Both the substitution of Fe for Co and addition of C elevated the T_c values, and in particular the effect of Co substitution was marked. The Curie temperature values for intermetallic compounds of rare earth and transition metal generally depend upon the magnitude of exchange interaction between transition metal atoms. The 3d band structure of transition metals is changed with increase of the Co content, and the increase of carbon content lengthens mainly Fe-Fe interatomic distance. In consequence, the exchange interaction

42

between transition metal atoms is enhanced and the T_c value is increased by Co substitution and carbon addition.

Figure 4.2 shows the magnetically aligned XRD patterns of $Sm_2(Fe_{1-x}Co_x)_{17}C_y$. It has been reported that the EMD of Sm_2Fe_{17} is in the basal plane[39], so that only (300) and (220) reflections are observed on the diffraction pattern (a). In the pattern of $Sm_2(Fe_{0.9}Co_{0.1})_{17}C_{0.1}$ (b), there were also only (300) and (220) reflections similarly to Sm_2Fe_{17}, and hence $Sm_2(Fe_{0.9}Co_{0.1})_{17}C_{0.1}$ has the c-plane anisotropy. The patterns (c) and (d) ($Sm_2(Fe_{0.9}Co_{0.1})_{17}C_{0.3}$ and $Sm_2(Fe_{0.7}Co_{0.3})_{17}C_{0.1}$) provided
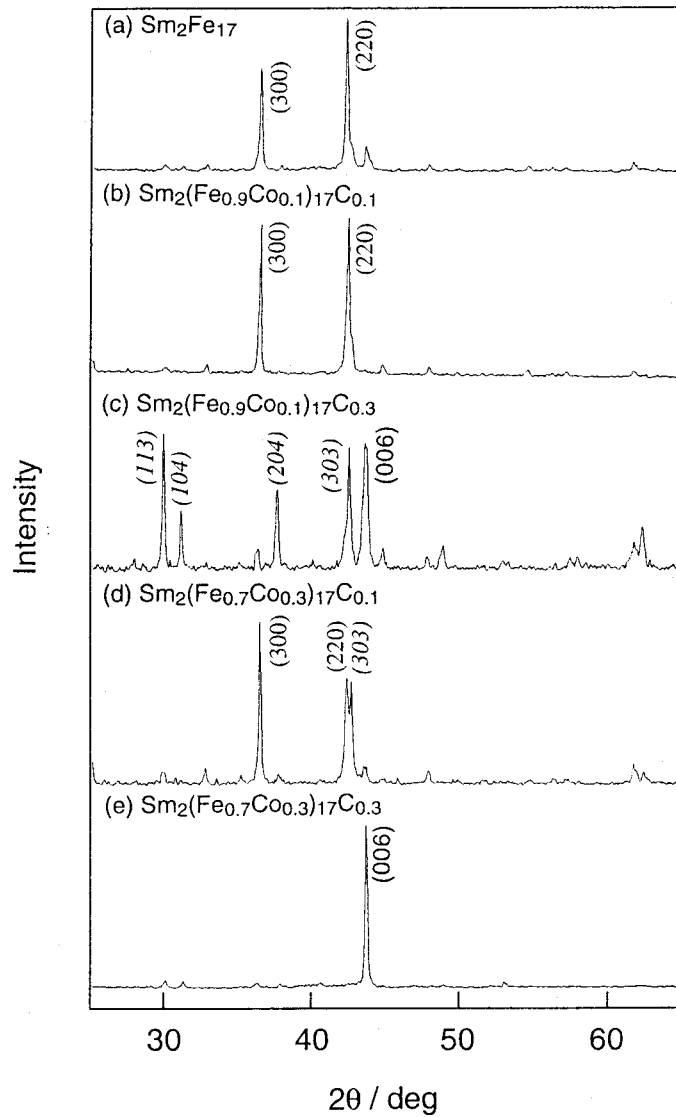

Figure 4.2. XRD patterns of the magnetically aligned $Sm_2(Fe_{1-x}Co_x)C_y$ samples.

(113), (104), (024) and (303) reflections in addition to (300) and (220) ones. This indicates that their EMDs are of the cone type. Whereas there is only the (303) reflection for $Sm_2(Fe_{0.7}Co_{0.3})_{17}C_{0.1}$, suggesting the cone anisotropy, the pattern of $Sm_2(Fe_{0.9}Co_{0.1})_{17}C_{0.3}$ has the (006) reflection in addition to the reflections which suggests the cone anisotropy. Therefore, it is estimated that the angle between EMD and the c-axis of $Sm_2(Fe_{0.9}Co_{0.1})_{17}C_{0.3}$ is smaller than that of $Sm_2(Fe_{0.7}Co_{0.3})_{17}C_{0.1}$.

Only (006) reflection was observed in pattern (e), and therefore the EMD of $Sm_2(Fe_{0.7}Co_{0.3})_{17}C_{0.3}$ was along the c-axis as were those of $Sm_2(Fe_{0.5}Co_{0.5})_{17}$ and $Sm_2Fe_{17}C_{0.5}$. According to a two-sublattice mean field model, the EMD of rare earth transition metal intermetallic compounds is determined by the competition between the EMDs of rare earth sublattice and transition metal sublattice. In the Th_2Zn_{17}-type crystal lattice, the Sm sublattice preferentially exhibits c-axis anisotropy because of the positive Stevens factor (α_J) of Sm atom, and the Fe sublattice contributes to the c-plane anisotropy. Consequently, although the role of both Co and carbon in $Sm_2(Fe_{1-x}Co_x)_{17}C_y$ compensates the contribution of Fe sublattice and makes the contribution of Sm sublattice dominant in the EMD competition, the effect of carbon is larger than that of Co.

The thermal stability of $Sm_2(Fe_{1-x}Co_x)_{17}C_y$ was decreased with the carbon content. This is due

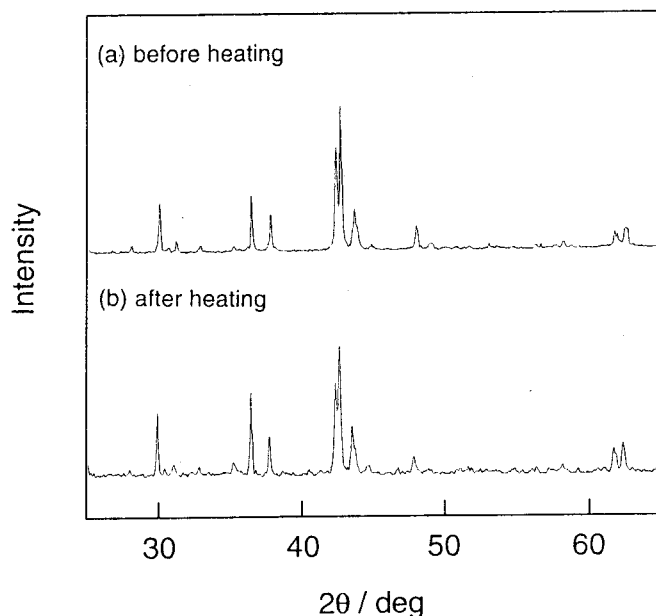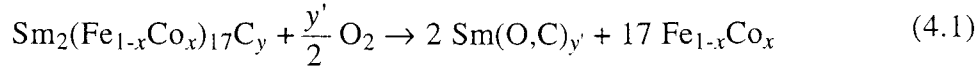**Figure 4.3.** XRD patterns of the $Sm_2(Fe_{1-x}Co_x)C_y$ samples (a) before and (b) after heating at 1300 K for 2 h.

44

to the formation of samarium oxycarbide and $Fe_{1-x}Co_x$ with the impurity of oxygen in the atmosphere used as shown in Eq. (4.1):

$$Sm_2(Fe_{1-x}Co_x)_{17}C_y + \frac{y'}{2} O_2 \rightarrow 2\ Sm(O,C)_{y'} + 17\ Fe_{1-x}Co_x \qquad (4.1)$$

However, the $Sm_2(Fe_{0.7}Co_{0.3})_{17}C_{0.3}$ powder (particle size = approx. 3 μm) was sintered at 1300 K in Ar without the above oxidation (see Fig 4.3).

4.4. Conclusions

The intermetallic compound $Sm_2(Fe_{0.7}Co_{0.3})_{17}C_{0.3}$ provided uniaxial anisotropy along the c-axis of the Th_2Zn_{17}-type structure, and furthermore its powder sample was sintered at 1300 K in Ar atmosphere without decomposition.

Chapter 5

Role of Interstitial Atoms in Magnetic Properties of $Sm_2Fe_{17}X_x$ (X = C or N)

5.1. Introduction

Due to the short Fe-Fe interatomic distance and their antiferromagnetic interaction, the Curie temperature of R_2Fe_{17} have been found quite low among all the R-Fe intermetallic compounds investigated so far. However, the T_c for those intermetallic compounds has been elevated drastically by the interstitial addition of carbon or nitrogen atoms. It is believed that the enhancement in magnetic properties of $R_2Fe_{17}X_x$ (X = C or N) was realized in such a way: the Fe-Fe interatomic exchange interaction was strengthened owing to the expansion in Fe-Fe interatomic distance initiated by the addition of interstitial carbon or nitrogen atoms. For related materials, several theoretical studies have been reported, for instance, the band-structure calculations on $Y_2Fe_{17}N_3$ by Jaswal et al.[40], using the self-consistent LMTO (linearized muffin-tin orbital) method[41], and those on $Nd_2Fe_{17}N_3$ by Gu and Lai[42], by means of the OLCAO (orthogonalized linear combination of atomic orbitals) band method. Min et al. have reported the electronic structure of $Sm_2Fe_{17}N_3$ employing LDA (local density-functional approximation) method with von BarthHedin formula for the exchange correlation interaction[43]. Unfortunately, $Y_2Fe_{17}N_3$, investigated by Jaswal et al., has a hexagonal Th_2Ni_{17} type crystal structure, which is different from that of $Sm_2Fe_{17}N_3$, and the OLCAO band results obtained by Gu and Lai were not self-consistently. Moreover, the atomic orbitals cannot be used as based functions in the method studied by Min et al.

In this chapter, electronic structures of $Sm_2Fe_{17}X_x$ (X = C or N) are estimated from DV-Xα molecular orbital calculation[44], and the role of the interstitial atoms in magnetic properties is discussed accordingly.

5.2. Experimental Details

The basis of DV-Xα molecular orbital calculation method is the self-consistent HFS (Hartree-Fock-Slater) model, on which the matrix elements of the Hamiltonian and overlap integrals were

calculated as weighted sums of values at discrete sample points, instead of the conventional integration procedure. The exchange-correlation term is given by a statistical local expression shown in Eq. (5.1):

$$V_{Xc_\sigma}(r) = -3\alpha[3\rho_\sigma(r) / 4\pi]^{1/3} \qquad (5.1)$$

where, $\rho(r)$, is the charge density at r; σ, the spin index (up or down); and, α, the only parameter used in this model fixed at 0.7. For each spin (up or down), we calculated the electronic structure using a one-electron Hamiltonian with the exchange-correlation term given in Eq. (5.1).

The model clusters with D_{6h} symmetry extracted from Sm_2Fe_{17}, $Sm_2Fe_{17}C_{2.5}$ and $Sm_2Fe_{17}N_{3.0}$ crystal lattice are shown in Fig. 5.1. The calculation was performed with 9000 DV sample points and used the basis orbital functions from 1s to 4p for Fe atom, from 1s to 2p for the C and N atoms. The radius and depth of the potential well are 3.5 Bohr units and -5.0 eV, respectively.
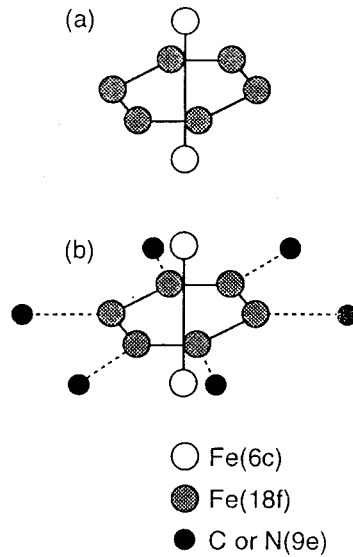

Figure 5.1. Structures of the clusters for calculation
(a) Fe_8 and (b) Fe_8C_6 or Fe_8N_6.

5.3. Results and Discussion

The charge and magnetic moment of Fe atoms in the clusters shown in Fig. 5.1(a) were listed in Table 5.1. The large calculated values of magnetic moments are obtained compared with experimental results reported elsewhere, because the electrons were localized at Fe atoms due to the restricted volume of the clusters. Since there are only Fe(6c) and Fe(18f) atoms in the clusters, it is possible for us to ascertain that the enhancement of the magnetic moment of Fe(6c) was based on an elongation of Fe-Fe interatomic distance. However, the ratio of the increase in magnetic moment was too small to explain the drastic elevation of T_c by carbidation or nitridation.

The charge and magnetic moment of the atoms in the clusters shown in Fig. 5.1(b) were tabulated in Table 5.2. The Fe atoms had positive charge because of the electron withdrawing effects from carbon and nitrogen atoms at 9e site, which have higher electronegativity than Fe. The charges of Fe(18f), which is the first neighbor of 9e sites, in the carbides and nitrides were different from each other. Because nitrogen is more electronegative than carbon, much more electrons of Fe(18f) in Fe_8N_6 clusters was withdrawn by nitrogen atoms compared with those in Fe_8C_6 cluster. On the contrary, the

Table 5.1. Charge (Q) and magnetic moment (μ) for Fe_8 clusters.

Compounds	Fe (6c)		Fe (18f)	
	Q	μ (μ_B)	Q	μ (μ_B)
Sm_2Fe_{17}	-0.038	3.352	+0.012	3.550
$Sm_2Fe_{17}C_{2.5}$	-0.041	3.353	+0.013	3.549
$Sm_2Fe_{17}N_{3.0}$	-0.040	3.354	+0.013	3.551

Table 5.2. Charge (Q) and magnetic moment (μ) for Fe_8C_6 and Fe_8N_6 clusters.

Compounds	Fe (6c)		Fe (18f)		N or C (9e)	
	Q	μ (μ_B)	Q	μ (μ_B)	Q	μ (μ_B)
$Sm_2Fe_{17}C_{2.5}$	+0.113	3.216	+0.060	3.282	-0.098	2.312
$Sm_2Fe_{17}N_{3.0}$	+0.111	3.356	+0.214	3.384	-0.252	2.164

charge of Fe(6c) atoms in these two different intermetallic compounds were almost equal to each other, as they were not efficiently influenced by interstitial carbon or nitrogen atoms because they were far from the 9e sites.

The magnetic moments of Fe(6c) atoms, however, are different from each other. Figure 5.2 shows the density of states (DOS) for both of the clusters. For the Fe_8N_6 cluster (Fig. 5.2(b)), the partial DOS for up spin of nitrogen atoms overlapped the partial DOS of Fe atoms under Fermi energy level, and the spin polarization were enhanced. On the other hand, the energy level of carbon atom is higher against the Fermi level than that of nitrogen atom and the DOS of up spin around the Fermi level are enhanced, so that the spin polarization were reduced. According to the spin-fluctuation theory by Mohn et al.[45], the Curie temperature is given by Eq. (5.2):
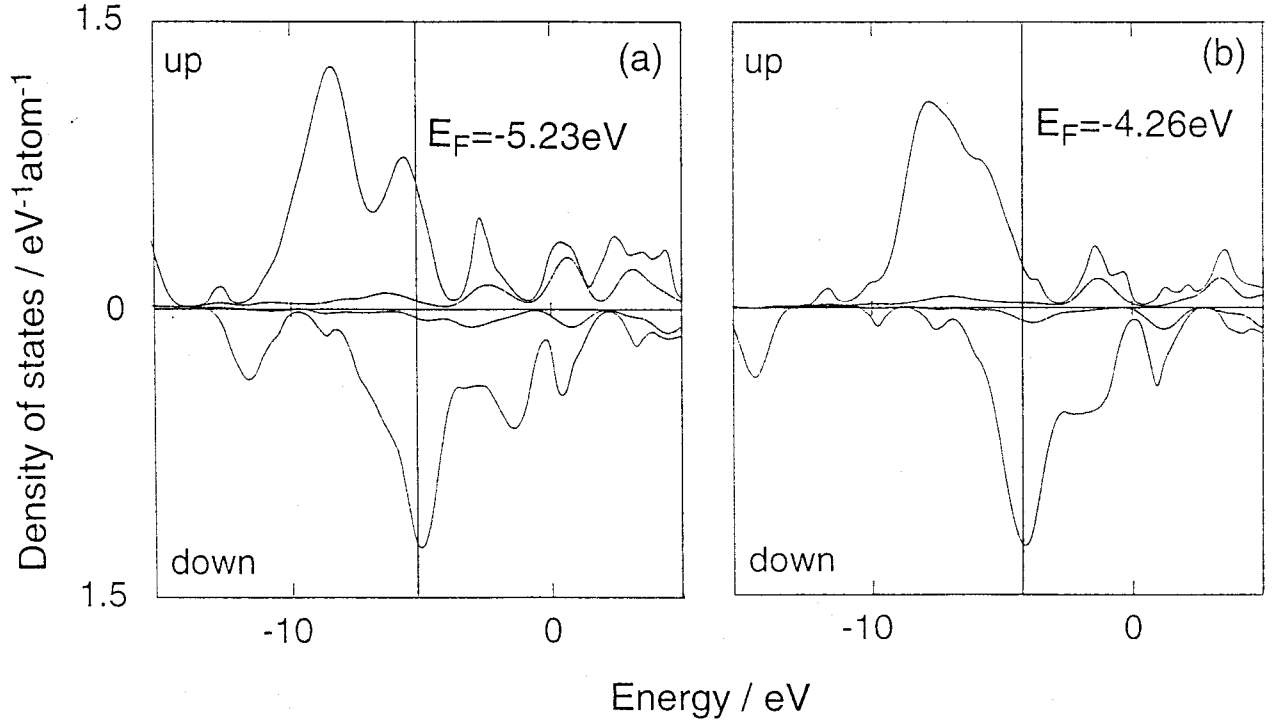
$$T_c \propto M_0^2 / \chi_0 \qquad\qquad (5.2)$$

Figure 5.2. Spin-polarized density of states for (a) Fe_8C_6 and (b) Fe_8N_6 clusters. (solid line: total density, dotted line: partial density of C or N).

49

where M_0 is the magnetic moment per atom at 0 K, and the enhanced susceptibility χ_0 is also given by Eq. (5.3):

$$\chi_0^{-1} = [\frac{1}{2} N_\uparrow(E_F)^{-1} + \frac{1}{2} N_\downarrow(E_F)^{-1} - I] / 2\mu_B^2 \qquad (5.3)$$

where, $N_\uparrow(E_F)$, and, $N_\downarrow(E_F)$, are the up and down spin DOS at the Fermi level; and, I, is the Stoner exchange energy. For the nitride, the magnetic moments of the Fe atoms are large and the DOS at the Fermi level are small compared with those for the carbide, hence the magnetization and Curie temperature of the nitride are higher than those of the carbide.

5.4. Conclusions

The magnetic moments of Fe(6c) atoms increased with an elongation of Fe-Fe interatomic distance by volume expansion of the unit cell. However, the increase effect is too small to explain the elevation of T_c or enhancement of magnetization. For the model cluster of $Sm_2Fe_{17}N_{3.0}$, the partially DOS of nitrogen atoms overlaps the DOS on Fe atoms, the spin polarization was thus enhanced.

Summary

In the work of this thesis, new preparation processes of rare earth-based permanent magnetic materials with high performance in magnetic properties and low production cost were described. The results obtained through this work are summarized as follows:

Chapter 1.

Although the direct reaction between rare earth dicarbides and transition metal could not lead to the formation of Th_2Zn_{17}-type or $ThMn_{12}$-type compounds, $Sm_2Fe_{17}C_x$ ($x < 1$) and $Nd(Fe,M)_{12}C_x$ ($x < 0.5$) have been obtained by use of RC_x ($x < 0.5$) as a source of rare earths and carbon. The further nitridation of $Sm_2Fe_{17}C_x$ provides the $Sm_2Fe_{17}C_xN_y$ compound which possesses good magnetic properties as well as the same material obtained by the conventional technique in which SmC_2 is not use as a starting material. The plasma nitridation performs efficiently compared with thermal nitridation for preparing $Nd(Fe,M)_{12}C_xN_y$. The T_c values of $Nd(Fe,M)_{12}X_x$ are dependent upon the corresponding unit cell volume and independent of the species of X element in a similar manner as observed on the $Nd(Fe,M)_{12}C_x$ and $Nd(Fe,M)_{12}N_x$ samples prepared by the conventional method. Therefore, the use of RC_2 as the starting material instead of rare earth metal and carbon may reduce the cost for the rare earth transition metal intermetallic carbonitrides.

Chapter 2.

It was found that the ball milling in an organic solution containing the surfactant was a suitable procedure for preparing the $Sm_2Fe_{17}N_x$ powder with excellent magnetic properties. For the powder obtained from this ball milling procedure, the particle size was uniform and the surface was smooth. In addition, the milling time to obtain enough H_{cj} value for practical use got shorter. The reasons of these are due to the addition of the surfactant, which suppresses the powder samples from aggregation to one another, or adhesion onto the surface of steel balls, and introduces of distortion into the particles. Each phenomenon may have an effect as follows: (1) uniformly ground powder leads to an improvement of rectangularity, (2) the smooth surface results in high coercivity because of reduction of nucleation

points and high resistivity against oxidation, (3) short milling time reduces the chance for the material to be oxidized. Therefore, the magnetic properties of the $Sm_2Fe_{17}N_x$ powder obtained here are considerably enhanced, and the huge BH_{max} value 330 kJm^{-3} is attained, consequently.

Chapter 3.

Zinc metal produced from photoinduced decomposition of $Zn(C_2H_5)_2$ by the chemical solution deposition (CSD) or chemical vapor deposition (CVD) method could be used to coat the surface of $Sm_2Fe_{17}N_x$ fine powder. The morphology of the zinc filmes coated by two methods are different from each other: the CSD samples had rough surface with some cracks, while the surface of the CVD sample was covered with a number of fine zinc particles. Although the magnetic properties of the $Sm_2Fe_{17}N_x$ fine powder have been changed a little by the zinc coating because of small content of non-magnetic zinc metal, the resistivity against oxidation of the powder is effectively improved through this process. The B_r, H_{cj} and BH_{max} values of zinc-coated $Sm_2Fe_{17}N_x$ ($Zn/Sm_2Fe_{17}N_x$) powder could be retained at high level after heat treatment in Ar atmosphere at 423 K for 10 h, however, the values of uncoated powder reduced markedly. When the temperature of heat treatment was raised over 523 K, the values of $Zn/Sm_2Fe_{17}N_x$ powder decreased.

The bonded magnet produced by use of $Zn/Sm_2Fe_{17}N_x$ powder gave the highest BH_{max} value (176 kJm^{-3}) among those reported by now. Furthermore, the BH_{max} value remained almost constant even after exposure to air at room temperature for 150 days.

Chapter 4.

Both substitution of Co for Fe and addition of carbon improved the magnetic properties of Sm_2Fe_{17}. The magnetization value of the $Sm_2(Fe_{1-x}Co_x)_{17}C_y$ increased with increase of Co content up to $x = 0.3$, which is reasonable since the magnetic moments of a series of $Fe_{1-x}Co_x$ alloys give a maximum around $x = 0.3$. The Curie temperature was elevated by both Co substitution and C addition, in particular, the former effect was dominant. $Sm_2(Fe_{0.7}Co_{0.3})_{17}C_{0.3}$ provided uniaxial anisotropy along the c-axis of the Th_2Zn_{17}-type structure, moreover, its powder sample was sintered at 1300 K in Ar atmosphere without decomposition.

52

Chapter 5.

Electronic states of the model clusters of Sm_2Fe_{17}, $Sm_2Fe_{17}C_{2.5}$ and $Sm_2Fe_{17}N_{3.0}$ have been calculated and orbital population was estimated by DV-$X\alpha$ molecular orbital calculation method. Magnetic moments of Fe atoms increase with expansion of the unit cell volume owning to addition of carbon and nitrogen atoms, but this increase effect is too small to explain the drastic elevation of T_c. For the model clusters of $Sm_2Fe_{17}C_{2.5}$ and $Sm_2Fe_{17}N_{3.0}$, the partially DOS of interstitial atoms overlap the DOS of Fe atoms and enhance the spin polarization, so that the Curie temperature and magnetic moment increase by carbidation or nitridation.

References

[1] M.Sagawa, S.Fujimura, N.Tagawa, H.Yamamoto and Y.Matsuura, *J.Appl.Phys.*, **55**, 2083 (1984).

[2] J.M.D.Coey and H.Sun, *J.Magn.Magn.Mater.*, **87**, L251 (1990).

[3] Y.Yang, Q.Pan, X.Zhang ang S.Ge, *J.Appl.Phys.*, **72**, 2989 (1992).

[4] Y.Yang, X.Zhang, L.Kong and Q Pan, *Solid State Commun.*, **78**, 317 (1991).

[5] M.Q.Huang, L.Y.Zhang, B.M.Ma, Y.Aheng, J.M.Elbicki, W.E.Walace and S.G.Sanker, *J.Appl.Phys.*, **70**, 6027 (1991).

[6] C.Kuhrt, K.O'Donnell, M.Katter, J.Wecker, K.Schnitzke and L.Schultz, *Appl.Phys.Lett.*, **60**, 3316 (1992).

[7] S.Suzuki and T.Miura, *IEEE Trans.Magn.*, **28**, 994 (1992).

[8] X.Kou, R.Grössinger, M.Katter, J.Wecker, L.Schults, T.H.Jacobs and K.H.J.Buschow, *J.Appl.Phys.*, **70**, 2272 (1991).

[9] X.Kou, R.Grössinger, X.Li, J.P.Liu, F.R.deBoer, M.Katter, J.Wecker, L.Schults, T. H.Jacobs and K.H.J.Buschow, *J.Appl.Phys.*, **73**, 6015 (1993).

[10] Z.Altounian, X.Chen, L.X.Liao, D.H.Ryan and J.O.Ström-Olsen, *J.Appl.Phys.*, **73**, 6017 (1993).

[11] K.Machida, Y.Nakatani, G.Adachi and A.Onodera, *Appl.Phys.Lett.*, **62**, 2874 (1993).

[12] K.Machida, A.Nakamoto and G.Adachi, *Chem.Mater.*, **6**, 2103 (1994).

[13] ASTM file of x-ray powder standards, *Inorganic Compounds*: SmC_2, 29-1115, ASTM, Philadelphia, PA.

[14] F.H.Spedding, K.Gschneidner,Jr. And A.H.Daane, *J.Am.Chem.Soc.*, **80**, 4499 (1958).

[15] G.Adachi, N.Imanaka and Z.Fuzhong, *Handbook on the Physics and Chemistry of Rare Earths*, eds. K.A.Gschneidner,Jr. And L.Eyring, Vol.15, p.61, Elsevier, Amsterdam, 1991.

[16] ASTM file of x-ray powder standards, *Inorganic Compounds*: Fe, 6-696, ASTM, Philadelphia, PA.

[17] W.Jeitschko and M.H.Gerss, *J.Less-Common Met.*, **116**, 147 (1986).

[18] M.H.Gerss, W.Jeitschko, L.Boonk, J.Nientiedt, E.Mörsen and A.Leson, *J.Solid State Chem.*, **70**, 19 (1987).

[19] H.H.Stadelmaier and H.K.Park, *Z.Metallkd.*, **72**, 417 (1981).

[20] Y.Otani, A.Moukarika, H.Sun, J.M.D.Coey, E.Devlin and I.R.Harris, *J.Appl.Phys.*, **69**, 6735 (1991).

[21] D.B.Booij and K.H.J.Buschow, *J.Less-Common Met.*, **142**, 249 (1988).

[22] Y.Yang, X.Zhang, S.Dong and Q.Pan, *J.Appl.Phys.*, **74**, 6847 (1993).

[23] K.H.J.Buschow, *Rep.Prog.Phys.*, **54**, 1123 (1991).

[24] K.Schnitzke, L.Schultz, J.Wecker and M.Katter, *Appl.Phys.Lett.*, **57**, 2853 (1990).

[25] R.Rani, H.Hedge, A.Navarathna and F.J.Cadien, *J.Appl.Phys.*, **73**, 6023 (1993).

[26] M.Katter, J.Wecker, C.Kuhrt, L.Schultz and R.Grössinger, *J.Magn.Magn.Mater.*, **117**, 419 (1992).

[27] X.Kou, W.Qiang, H.Kronmüller and L.Schultz, *J.Appl.Phys.*, **74**, 6791 (1993).

[28] H.Li and J.M.D.Coey, *Handbook of Magnetic Materials*, Vol. 6, p.46, ed. K.H.J.Buschow, North-Holland, Tokyo, 1991.

[29] T.Mukai and T.Fujimoto, *J.Magn.Magn.Mater.*, **103**, 165 (1990).

[30] K.Kobayashi, T.Iriyama, T.Yamaguchi, H.Kato and Y.Nakagawa, *J.Alloys Compd.*, **193**, 235 (1993).

[31] S.Tajima, T.Hattori and Y.Kato, *J.Magn.Soc.Jpn.*, **19**, 221 (1995) in Japanese.

[32] K.Hiraga, K.Okamoto and T.Iriyama, *Mater.Transitions JIM*, **34**, 569 (1993).

[33] N.Imaoka and T.Iriyama, *Denkigakkai-Kenkyukai-Shiryo*, **Mag-95-54**, 27 (1995) in Japanese.

[34] T.Iriyama, T.Katsumata and R.Mitsui, *Trans.Mat.Res.Soc.Jpn.*, **14B**, 1063 (1994).

[35] D.B.deMooij and K.H.J.Buschow, *J.Less-Common Met.*, **142**, 349 (1988).

[36] W.G.Haije, T.H.Jacobs and K.H.J.Buschow, *J.Less-Common Met.*, **163**, 353 (1990).

[37] M.Katter, J.Wecker, C.Kuhrt and L.Schultz, *J.Magn.Magn.Mater.*, **114**, 35 (1992).

[38] H.Li and J.M.D.Coey, *Handbook of Magnetic Materials*, Vol. 6, p.43, ed. K.H.J.Buschow, North-Holland, Tokyo, 1991.

[39] H.R.Kirchmayr and C.A.Poldy, *Handbook on the Physics and Chemistry of Rare Earths*, eds. K.A.Gschneidner,Jr. and L.Eyring, Vol. 2, p. 155, North-Holland, Amsterdam, 1979.

[40] S.S.Jaswell, W.B.Yelon, G.C.Hadjipanayis, Y.Z.Wang and D.J.Sellmyer, *Phys.Rev.Lett.*, **67**, 644 (1992).

[41] O.K.Anderson, *Phys.Rev.B*, **12**, 3060 (1975).

[42] Z.Gu and W.Lai, *J.Appl.Phys.*, **71**, 3911 (1992).

[43] B.Min, J.Kang, J.Hong, S.Jung, J.Jeong, Y.Lee. S.Choi, W.Lee, C.Yang and C.Olson, *J.Phys.:Condens.Matter*, **5**, 6911 (1991).

[44] H.Adachi, M.Tsukada and C.Satoko, *J.Phys.Soc.Jpn.*, **45**, 875 (1978).

[45] P.Mohn and E.P.Wohlfarth, *J.Phys.*, **F17**, 2421 (1987).

Acknowledgments